Human Brain Mapping

WILEY

RESEARCH ARTICLE OPEN ACCESS

Grey-Matter Structure Markers of Alzheimer's Disease, Alzheimer's Conversion, Functioning and Cognition: A Meta-Analysis Across 11 Cohorts

Baptiste Couvy-Duchesne[1,2] | Vincent Frouin[3] | Vincent Bouteloup[4] | Nikitas Koussis[5,6] | Julia Sidorenko[1] | Jiyang Jiang[7] | Alle Meije Wink[8,9] | Luigi Lorenzini[8,9] | Frederik Barkhof[8,10] | Julian N. Trollor[11] | Jean-François Mangin[3] | Perminder S. Sachdev[7,12] | Henry Brodaty[7] | Michelle K. Lupton[13,14,15] | Michael Breakspear[5,6] | Olivier Colliot[2] | Peter M. Visscher[1,16] | Naomi R. Wray[1,17] | for the Alzheimer's Disease Neuroimaging Initiative | the Australian Imaging Biomarkers and Lifestyle flagship study of ageing | the Alzheimer's Disease Repository Without Borders Investigators | the MEMENTO cohort Study Group

[1]Institute for Molecular Bioscience, The University of Queensland, St Lucia, Queensland, Australia | [2]Paris Brain Institute – ICM, CNRS, Inria, Inserm, AP-HP, Hôpital de la Pitié Salpêtrière, Sorbonne University, Paris, France | [3]CEA, CNRS, Neurospin, Baobab, Paris-Saclay University, Saclay, France | [4]Univ. Bordeaux, Inserm, Bordeaux Population Health, UMR1219, CIC 1401 EC, Pôle Santé Publique, CHU de Bordeaux, Bordeaux, France | [5]School of Psychological Sciences, The University of Newcastle, Callaghan, New South Wales, Australia | [6]Hunter Medical Research Institute, Newcastle, New South Wales, Australia | [7]Centre for Healthy Brain Ageing, Discipline of Psychiatry & Mental Health, School of Clinical Medicine, Faculty of Medicine and Health, University of New South Wales, Sydney, New South Wales, Australia | [8]Department of Radiology and Nuclear Medicine, Amsterdam UMC, Vrije Universiteit, Amsterdam, The Netherlands | [9]Amsterdam Neuroscience, Brain Imaging, Amsterdam, The Netherlands | [10]Queen Square Institute of Neurology and Centre for Medical Image Computing, University College London, London, UK | [11]Department of Developmental Disability Neuropsychiatry, School of Clinical Medicine, UNSW, Sydney, New South Wales, Australia | [12]Neuropsychiatric Institute, Prince of Wales Hospital, Sydney, New South Wales, Australia | [13]QIMR Berghofer Medical Research Institute, Brisbane, Queensland, Australia | [14]School of Biomedical Sciences, Faculty of Medicine, The University of Queensland, Brisbane, Queensland, Australia | [15]School of Biomedical Sciences, Faculty of Health, Queensland University of Technology, Brisbane, Queensland, Australia | [16]Nuffield Department of Population Health, University of Oxford, Oxford, UK | [17]Department of Psychiatry, University of Oxford, Oxford, UK

Correspondence: Baptiste Couvy-Duchesne (b.couvyduchesne@uq.edu.au)

Received: 10 March 2024 | **Revised:** 6 November 2024 | **Accepted:** 17 November 2024

Funding: This research was supported by the Australian National Health and Medical Research Council (1078037, 1078901, 1113400, 1161356 and 1107258), the Australian Research Council (FT180100186 and FL180100072), the Sylvia & Charles Viertel Charitable Foundation, the program 'Investissements d'avenir' ANR-10-IAIHU-06 (Agence Nationale de la Recherche-10-IA Institut Hospitalo-Universitaire-6) and reference ANR-19-P3IA-0001 (PRAIRIE 3IA Institute), the European Union H2020 program (project EuroPOND, grant number 666992), the joint NSF/NIH/ANR program 'Collaborative Research in Computational Neuroscience' (project HIPLAY7, grant number ANR-16-NEUC-0001-01), the ICM Big Brain Theory Program (project DYNAMO, project PredictICD), and the Abeona Foundation (project Brain@Scale). The ADNI data collection and sharing was funded by the Alzheimer's Disease Neuroimaging Initiative (ADNI) (National Institutes of Health Grant U01 AG024904) and DOD ADNI (Department of Defense award number W81XWH-12-2-0012). ADNI is funded by the National Institute on Aging, the National Institute of Biomedical Imaging and Bioengineering, and

Olivier Colliot, Peter M. Visscher, and Naomi R. Wray contributed equally to this study.

The Alzheimer's Disease Neuroimaging Initiative: Data used in preparation of this article were obtained from the Alzheimer's Disease Neuroimaging Initiative (ADNI) database (adni.loni.usc.edu). As such, the investigators within the ADNI contributed to the design and implementation of ADNI and/or provided data but did not participate in analysis or writing of this report. A complete listing of ADNI investigators can be found at: http://adni.loni.usc.edu/wp-content/uploads/how_to_apply/ADNI_Acknowledgement_List.pdf.

The Australian Imaging Biomarkers and Lifestyle flagship study of ageing: Data used in the preparation of this article was obtained from the Australian Imaging Biomarkers and Lifestyle flagship study of ageing (AIBL) funded by the Commonwealth Scientific and Industrial Research Organisation (CSIRO) which was made available at the ADNI database (www.loni.usc.edu/ADNI). The AIBL researchers contributed data but did not participate in analysis or writing of this report. AIBL researchers are listed at www.aibl.csiro.au.

The Alzheimer's Disease Repository Without Borders Investigators: Data used in preparation of this article were obtained from the Alzheimer's Disease Repository Without Borders (ARWiBo) database (www.arwibo.it). As such, the researchers within the ARWiBo contributed to the design and implementation of ARWiBo and/or provided data but did not participate in analysis or writing of this report. A complete listing of ARWiBo researchers can be found at: www.arwibo.it/acknowledgement.it.

The MEMENTO cohort Study Group: Data used in preparation of this article were obtained from the MEMENTO Cohort (http://www.memento-cohort.org/). Access to the MEMENTO database was managed through the Dementia Platform in UK (https://portal.dementiasplatform.uk/). VB and VF, from the MEMENTO Cohort team, participated to the writing of this report.

through generous contributions from the following: AbbVie, Alzheimer's Association; Alzheimer's Drug Discovery Foundation; Araclon Biotech; BioClinica, Inc.; Biogen; Bristol-Myers Squibb Company; CereSpir, Inc.; Cogstate; Eisai Inc.; Elan Pharmaceuticals, Inc.; Eli Lilly and Company; EuroImmun; F. Hoffmann-La Roche Ltd. and its affiliated company Genentech, Inc.; Fujirebio; GE Healthcare; IXICO Ltd.;Janssen Alzheimer Immunotherapy Research & Development, LLC.; Johnson & Johnson Pharmaceutical Research & Development LLC.; Lumosity; Lundbeck; Merck & Co., Inc.; Meso Scale Diagnostics, LLC.; NeuroRx Research; Neurotrack Technologies; Novartis Pharmaceuticals Corporation; Pfizer Inc.; Piramal Imaging; Servier; Takeda Pharmaceutical Company; and Transition Therapeutics. The Canadian Institutes of Health Research is providing funds to support ADNI clinical sites in Canada. Private sector contributions are facilitated by the Foundation for the National Institutes of Health (www.fnih.org). The grantee organisation is the Northern California Institute for Research and Education, and the study is coordinated by the Alzheimer's Therapeutic Research Institute at the University of Southern California. ADNI data are disseminated by the Laboratory for Neuro Imaging at the University of Southern California. AIBL funding for the study was provided by CSIRO, which was supplemented by 'in kind' contributions from the study partners. The study also received support from the National Health and Medical Research Council via the Dementia Collaborative Research Centres program (DCRC2). ARWIBO data collection and sharing for this project was supported by the Italian Ministry of Health, under the following grant agreements: Ricerca Corrente IRCCS Fatebenefratelli, Linea di Ricerca 2; Progetto Finalizzato Strategico 2000–2001 'Archivio normativo italiano di morfometria cerebrale con risonanza magnetica (età 40+)'; Progetto Finalizzato Strategico 2000–2001 'Decadimento cognitivo lieve non dementigeno: stadio preclinico di malattia di Alzheimer e demenza vascolare. Caratterizzazione clinica, strumentale, genetica e neurobiologica e sviluppo di criteri diagnostici utilizzabili nella realtà nazionale'; Progetto Finalizzata 2002 'Sviluppo di indicatori di danno cerebrovascolare clinicamente significativo alla risonanza magnetica strutturale'; Progetto Fondazione CARIPLO 2005–2007 'Geni di suscettibilità per gli endofenotipi associati a malattie psichiatriche e dementigene'; 'Fitness and Solidarietà'; and anonymous donors. The EPAD was funded by the EU/The European Federation of Pharmaceutical Industries and Associations (EFPIA) Innovative Medicines Initiative Joint Undertaking (grant agreement 115736). FB and AMW receive funding from the Alzheimer's Disease Data Initiative (ADDI, www.alzheimersdata.org) project, a 501(c)(3) Medical Research Organisation (USA). FB is supported by the NIHR biomedical research centre at UCLH. The MAS study and data collection was supported by the Australian National Health and Medical Research Council (NHMRC) Program Grants (ID No. ID350833, ID568969, and APP1093083). MRI scans were processed with the support of NHMRC Project Grants (510175 and 1025243) and an ARC Discovery Project Grant (DP0774213) and John Holden Family Foundation. We also thank the MRI Facility at NeuRA. The MEMENTO cohort is funded by the Fondation Plan Alzheimer (Alzheimer Plan 2008–2012), through the Plan Maladies Neurodégénératives (2014–2019), and the French Ministry of Research (MESRI, DGRI 2020–2024). This work was also supported by CIC 1401-EC, Bordeaux University Hospital (CHU Bordeaux, sponsor of the cohort), Inserm, and the University of Bordeaux. The MEMENTO cohort has received funding support from AVID, GE Healthcare, and FUJIREBIO through private–public partnerships. The OASIS3 data were provided by Principal Investigators: T. Benzinger, D. Marcus, J. Morris supported by NIH grants: P50AG00561, P30NS09857781, P01AG026276, P01AG003991, R01AG043434, UL1TR000448, R01EB009352. The OATS (Older Australian Twins Study) was supported by the National Health and Medical Research Council (NHMRC) & Research Council (ARC) Strategic Award Grant of the Ageing Well, Ageing Productively Program (grant 401162); NHMRC Project (seed) Grants (ID No. 1024224 and 1025243); NHMRC Project Grants (ID No. 1045325 and 1085606); and NHMRC Program Grants (ID No. 568969 and 1093083). The Australian Twin Registry is supported by a Centre of Research Excellence Grant from the NHMRC administered by the University of Melbourne. PISA data collection was funded by an NHMRC Boosting Dementia Research Initiative—Team Grant (APP1095227).

ABSTRACT

Alzheimer's disease (AD) brain markers are needed to select people with early-stage AD for clinical trials and as quantitative endpoint measures in trials. Using 10 clinical cohorts ($N = 9140$) and the community volunteer UK Biobank ($N = 37{,}664$) we performed region of interest (ROI) and vertex-wise analyses of grey-matter structure (thickness, surface area and volume). We identified 94 trait-ROI significant associations, and 307 distinct cluster of vertex-associations, which partly overlap the ROI associations. For AD versus controls, smaller hippocampus, amygdala and of the medial temporal lobe (fusiform and parahippocampal gyri) was confirmed and the vertex-wise results provided unprecedented localisation of some of the associated region. We replicated AD associated differences in several subcortical (putamen, accumbens) and cortical regions (inferior parietal, postcentral, middle temporal, transverse temporal, inferior temporal, paracentral, superior frontal). These grey-matter regions and their relative effect sizes can help refine our understanding of the brain regions that may drive or precede the widespread brain atrophy observed in AD. An AD grey-matter score evaluated in independent cohorts was significantly associated with cognition, MCI status, AD conversion (progression from cognitively normal or MCI to AD), genetic risk, and tau concentration in individuals with none or mild cognitive impairments (AUC in 0.54–0.70, p-value $< 5e\text{-}4$). In addition, some of the grey-matter regions associated with cognitive impairment, progression to AD ('conversion'), and cognition/functional scores were also associated with AD, which sheds light on the grey-matter markers of disease stages, and their relationship with cognitive or functional impairment. Our multi-cohort approach provides robust and fine-grained maps the grey-matter structures associated with AD, symptoms, and progression, and calls for even larger initiatives to unveil the full complexity of grey-matter structure in AD.

1 | Introduction

Research into Alzheimer's disease (AD) aetiology suggests that the underlying neuropathology (toxic amyloid-β [Aβ] species and hyperphosphorylated tau protein accumulation) can be observed many years (possibly decades) before the first symptoms of cognitive or functional decline (Jack et al. 2010; Villemagne et al. 2013). Accumulation of Aβ and tau is thought to result in synaptic, neuronal and axonal damage, leading to grey-matter atrophy, typically seen first in the hippocampus and medial temporal lobe (Frisoni et al. 2010; Jack et al. 2010). These brain changes progressively tap into the 'brain reserve' (Fratiglioni and Wang 2007), which could explain the delay between brain atrophy and onset of mild cognitive impairment, which itself can precede AD diagnosis by a few years (Apostolova 2016; Frisoni et al. 2010; Jack et al. 2010).

Recent clinical trials testing new drugs for AD focus on individuals with early AD (mild cognitive impairment or mild dementia) (van Dyck et al. 2023). Hence, AD imaging biomarkers are needed to improve disease staging (Matsuda 2016), identify trial participants, and could also serve as secondary endpoints in trials to evaluate the effect of treatment/intervention on the brain (van Dyck et al. 2023). In research, brain biomarkers may be used to study AD risk in cohorts where the information was not collected or available, and to prioritise the disease-relevant brain regions in molecular analyses (e.g., omics).

PET (positron emission tomography) is considered the brain imaging modality of choice for Alzheimer's in that it can measure Aβ, tau or fluorodeoxyglucose (synaptic dysfunction) (Jack et al. 2010). However, the radiochemistry availability and cost limit its use in research and the number of scans available. In comparison, structural MRI (sMRI) can provide biomarkers of early AD, is less invasive and leverages scans that have been extensively collected in both clinical and research settings. In addition, sMRI can capture grey-matter changes regardless of the underlying neuropathological processes and is hence potentially more sensitive (Bejanin et al. 2017; Chételat et al. 2010; Frisoni et al. 2009).

Several studies have identified brain regions more susceptible to grey-matter atrophy in Alzheimer's disease. Early atrophy of hippocampus, amygdala and medial temporal lobe (entorhinal, parahippocampus gyri) has been well documented, and even confirmed by neuronal counts in autopsies (Johnson et al. 2012). Atrophy has also been reported in the posterior cingulate, precuneus and in the rest of the temporal lobe, or in the sensory and primary motor cortex although they are thought to appear later in the disease progression (Johnson et al. 2012; van Oostveen and de Lange 2021). However, most of these neuroimaging studies have relied on a single neuroimaging cohort and the reported levels of regional atrophy vary widely from one study to the next (e.g., hippocampal reduction reported between 15% and 25%, yearly rate of atrophy between 3% and 5%) (Johnson et al. 2012), which may reflect different disease severity or stages in the sample, but may also reflect a lack of precision of the effect sizes estimated from small samples (Marek et al. 2022). In addition, there is currently no multi-cohort agnostic study of structural AD brain markers (e.g., similar to that of the ENIGMA consortium Thompson et al. 2020), that can quantify the relative associations of the different brain regions, provide robust maps of associations (generalizable to other cohorts) and detect novel associations by boosting statistical power (Marek et al. 2022; Smith and Nichols 2018). To answer this challenge, we have gathered almost 10,000 scans from 10 clinical cohorts (and > 37,000 from the UK Biobank), to perform exploratory analyses of brain markers of Alzheimer's disease. We have used the ENIGMA processing pipelines to extract grey-matter measurements to make our results comparable with those obtained by the consortium on other disorders of the brain (Thompson et al. 2020).

Neuroimaging studies of AD progression from MCI or cognitively normal (CN) (and more generally of early stages of AD) can shed light on early brain markers, which are of greater clinical interest. However, they are limited by small sample sizes that reflect the difficulty, and cost associated with following individuals prospectively, over years. As a consequence, only the hippocampus and entorhinal cortex have been confidently linked to Alzheimer's conversion (i.e., progression from MCI or CN to AD related dementia) (Lombardi et al. 2020), and predictors based on brain structure currently exhibit low robustness and performance (Ansart et al. 2021). Here, we combined data from several cohorts, to directly investigate the structural brain markers associated with MCI status, Alzheimer's conversion, as well as neuropsychological (cognition and functioning) scores. In addition, we systematically evaluated the (out-of-sample) prediction accuracy achieved from the identified biomarkers of Alzheimer's disease course and quantify their generalizability and possible usage in research or clinical trials.

Another limitation of the brain biomarkers identified to date is that they comprise broad brain regions or structures (regions of interest [ROI]) which lack precision or specificity. For example, the medial temporal lobe atrophy reported, does not precisely identify the atrophied gyri or the contours of the susceptible region(s). Lower hippocampal volume in AD is well established, and may originate in the CA1 subfield (de Flores, La Joie, and Chételat 2015), although it is also observed across most subfields (Zhang et al. 2023). More precise association maps (at a voxel/vertex wise level) are needed, that could reveal disease specific signatures in grey-matter structure, beyond the reduction in hippocampal volume (and subfields) that have been found for most diseases studied by the ENIGMA (Enhancing Neuro-Imaging Genetics through Meta-Analysis) consortium (Thompson et al. 2020). To progress this issue, we complemented our ROI based analyses by brain wide association studies at a vertex level. The large samples sizes we gathered provides improved statistical power to detect significant brain regions, despite the high multiple testing correction (Smith and Nichols 2018). Vertex-wise measurements capture more of the grey-matter complexity, than ROI measurements (Couvy-Duchesne, Strike, et al. 2020; Fürtjes et al. 2023), which should pave the way to more performant brain based predictors (Couvy-Duchesne, Strike, et al. 2020).

In our primary analysis, we performed a multi-cohort investigation of grey-matter structure associated with Alzheimer's disease. Our project complements the current ENIGMA initiatives (Thompson et al. 2020) by extending the analyses to Alzheimer's disease. In addition to a Region of Interest (ROI) approach, we perform analyses at a vertex level, to identify more localised brain markers, that could be more disease specific and predictive (Couvy-Duchesne, Strike, et al. 2020; Couvy-Duchesne et al. 2022). To ensure robust results, we systematically evaluated replication and out-of-sample prediction that the brain markers can achieve (Couvy-Duchesne et al. 2022; Marek et al. 2022). Finally, in a secondary analysis, we investigated the grey-matter associations with several disease stages (MCI, conversion), symptoms (cognition, functioning) and AD risk (family history). Together, primary and secondary analyses can help identify converging brain biomarkers and evaluate how they translate into risk prediction across disease stages.

2 | Material and Methods

2.1 | Samples

Data from 11 cohorts of older adults that collected structural brain MRI (T1w) were used together with clinical information or neuropsychological scores of interests (Table 1, see Appendix A and Table S1, for details). We included data from ADNI (Alzheimer's Disease Neuroimaging Initiative, which we split in two cohorts ADNI1 and ADNI2 + GO + 3, based on MRI scanners [1.5T vs. 3T]), AIBL (Australian Imaging, Biomarker and Lifestyle) (Ellis et al. 2009), ARWIBO (Alzheimer's Disease Repository Without Borders) (Frisoni et al. 2020; Riello et al. 2005), EPAD (European Prevention of Alzheimer's Dementia) (Lorenzini et al. 2021; Ritchie et al. 2020; Solomon et al. 2019), MAS (Sydney Memory and Ageing Study) (Kochan et al. 2010; Sachdev et al. 2010; Tsang et al. 2013), OASIS3 (Open Access Series of Imaging Studies 3) (LaMontagne et al. 2018), OATS (Older Adults Twin Study) (Koncz et al. 2018; Sachdev et al. 2009, 2013), MEMENTO (Dufouil et al. 2017) and PISA (Prospective Imaging Study of Ageing: Genes, Brain and Behaviour) (Lupton et al. 2020) and the UK Biobank (Miller et al. 2016).

We used ADNI1, ADNI2GO3, AIBL, ARWIBO, EPAD, MAS, OASIS3 and OATS as discovery samples, which together comprise 6981 individuals with usable brain MRI, including 4653 healthy controls at the time of MRI, 1343 individuals with mild cognitive impairment (MCI) and 796 Alzheimer's disease cases (Table 1). We sought to replicate the findings in MEMENTO ($N = 1880$) and PISA ($N = 279$). The UK Biobank is, by far, the largest neuroimaging study ($N = 37{,}644$), but due to the recruitment strategy (community volunteer, and age range) there were no AD cases at the time of imaging, and only a handful of incident cases had been reported at the time of data extraction. Thus, we only used the UKB in our analyses of parental history (Appendix A, Table 1, Table S1).

2.2 | Clinical Status and Traits of Interest

We tested for differences in grey-matter structure of individuals with Alzheimer's disease to that of healthy controls (AD versus HC) and MCI (AD versus MCI), and between MCI and controls (MCI versus HC). We also used a 3-point scale: 0 = HC, 1 = MCI, 2 = AD.

We studied AD conversion (or progression to AD dementia) using participants who were recorded as controls and MCI individuals at the time of brain imaging but who later received a diagnosis of Alzheimer's disease and considered different post-imaging time frames (1, 2, 3, 4 and 5 years). We ensured that non-converter individuals had been also followed over the same time window.

We studied neuropsychological scales that were available in at least 4 out of the 8 discovery cohorts or that were available on more than 3000 individuals. Thus, we considered scores from the Mini Mental Scale Evaluation (MMSE, available on all cohorts), Clinical Dementia Rating (CDR), Functional Activity Questionnaire (FAQ) that assess dementia symptoms and functioning. We also included the Geriatric Depression Scale (GDS) and the Neuropsychiatric Inventory Questionnaire (NPI-Q) that focus on the psychiatric domains often associated with Alzheimer's. In addition, we studied memory scores such as the Rey Auditory Verbal Learning Test (RAVLT) which produces 5 scores of verbal memory (short term memory, working memory and long-term memory), and the Logical Memory scores that target episodic memory (short and long term).

Lastly, we considered self-reported maternal and paternal history of Alzheimer's disease. Parental history is available on the UK Biobank and could serve as a proxy phenotype for Alzheimer's disease in samples that do not contain many cases (Marioni et al. 2018).

2.3 | MRI Acquisition and Processing

We have summarised the MRI acquisition parameters used in the different studies in Appendix A. For all samples (except for the UKB), we performed the surface based processing of the T1w brain MRI using FreeSurfer 6.0 (Fischl 2012), followed by the ENIGMA-shape package (https://enigma.ini.usc.edu/ongoing/enigma-shape-analysis/) (Gutman et al. 2013; Gutman et al. 2012).

For the UKB, we downloaded the outputs from FreeSurfer 6.0 processing performed by the UKB (bulk field 20,263), which used the T1w but also the T2 Flair images in order to improve grey-matter parcellation (Miller et al. 2016). We then conducted the ENIGMA-shape processing, to further extract surface-based processing of seven subcortical structures.

2.4 | ROI and Vertex-Wise Grey-Matter Measurements

We extracted the Region of Interest (ROI) values (produced by FreeSurfer 6.0), of cortical thickness and surface area based on the Desikan-Killiany atlas (Desikan et al. 2006), as well as the volume of the seven subcortical structures. This resulted in 150 ROI measurements of grey-matter structure, which correspond to the brain measurements used in previous ENIGMA publications (Thompson et al. 2020). Mean and variances of the ROI based measurements were comparable between samples, that were acquired on different machines (Figure S1).

In addition, we extracted 654,002 vertex-wise measurements, which consist in 299,881 cortical vertices ('fsaverage mesh') for which we have thickness and surface area measurements and 27,120 subcortical vertices, at which we measure radial thickness and a measure analogous to a surface area (Roshchupkin et al. 2016). We have used and evaluated this MRI processing in two previous publications (Couvy-Duchesne, Zhang, et al. 2020; Couvy-Duchesne et al. 2021).

Using the standardised vertex-wise measurements, we calculated the brain-relatedness matrix for each sample, which quantifies the similarities between a pair of individuals' grey-matter structure (Couvy-Duchesne, Strike, et al. 2020). We excluded the pairs of participants that had the extremely similar or dissimilar

TABLE 1 | Summary of the cohorts used in the analyses.

	Sample (field strength and scanner)	*N*	Age Mean (SD)	Sex *N* female (%)	AD *N* (%)	MCI *N* (%)	HC[b] *N* (%)	Other data
Discovery	ADNI1 (1.5T; GE, Philips, Siemens)	805	75.2 (6.8)	465 (57.8%)	186 (23.0%)	393 (49.0%)	226 (28.0%)	Conversion (15 years); MMSE; CDR; FAQ; GDS; NPI-Q; RAVLT; Logical Memory; Family history
	ADNI2GO3 (3T; GE, Philips, Siemens)	1,410	72.1 (7.19)	733 (50.3%)	195 (13.8%)	619 (43.9%)	577 (41.0%)	Conversion (1–5 years); MMSE; CDR; FAQ; GDS; NPI-Q; RAVLT; Logical Memory; Family history
	AIBL (1.5 and 3T; Siemens)	606	72.8 (6.7)	335 (55.3%)	72 (11.9%)	89 (14.7%)	443 (73.1%)	Conversion (15 years)[a]; MMSE; CDR; Logical Memory
	ARWIBO (1 and 1.5T; GE, Philips, Siemens)	934	56.7 (16.0)	565 (60.5%)	130 (13.9%)	0 (0%)	715 (76.6%)	MMSE; CDR; Family History
	EPAD (1.5 and 3T; GE, Philips, Siemens)	1315	64.4 (7.1)	748 (56.8%)	0 (0%)	0 (0%)	1315 (100%)	Conversion (1–3 years); MMSE; CDR; GDS; Family History
	MAS (3T; Philips)	527	78.4 (4.7)	290 (55.0%)	0 (0%)	175 (33.2%)	288 (54.6%)	Conversion (2–5 years); MMSE; CDR; RAVLT; Logical memory
	OASIS3 (1.5 and 3T; Siemens)	1019	70.7 (9.3)	565 (55.4%)	207 (20.3%)	21 (0.02%)	791 (77.6%)	Conversion (1–5 years); MMSE; CDR; GDS; NPI-Q; Logical Memory; Family History
	OATS (1.5T; Philips, Siemens)	365	70.3 (5.1)	240 (65.8%)	6 (1.4%)	46 (12.6%)	308 (84.4%)	Conversion (2–5 years)[a]; MMSE; GDS; NPI-Q; RAVLT; Logical Memory
	UKB (3T; Siemens)	37,664	63.6 (7.5)	20,056 (53.3%)	0 (0%)	0 (0%)	37,664 (100%)	Conversion (2–10 years)[a]; Family history
Replication	MEMENTO (1.5 and 3T; GE, Philips, Siemens)	1,880	70.0 (8.7)	1199 (63.8%)	0 (0%)	1575 (83.8%)	305 (16.2%)	Conversion (1–5 years); MMSE; CDR, IADL (proxy for FAQ), DMS48 (proxy for logical memory scores)
	PISA (3T; Siemens)	279	60.6 (6.9)	193 (72.3%)	26 (9.7%)	21 (7.9%)	220 (82.4%)	RAVLT

[a]Denotes that numbers were too small to be used in meta-analyses.
[b]We defined as 'healthy controls' individuals without a diagnosis of AD or MCI, but they may differ between cohorts according to the recruitment strategies and screening. For example, MEMENTO recruited in memory clinics, and all HC have subjective cognitive decline, while ARWIBO controls were screened for a range of neurodegenerative disorders. See Appendix A for more details.

grey-matter (8SD from the distribution mean), as they can bias results from mixed model analyses. This led to exclusion of between 0.3% and 0.9% of the individuals across the different samples.

As a check of compatibility of the different datasets, we contrasted the mean and variance of the vertex-wise measurements calculated on the healthy individuals from the different samples (Figures S2–S5). We observed a great concordance of the average vertex values across the different samples. Of note, average cortical thickness was larger in the UKB (Figure S3) than in the other samples, which is a known consequence of the combined use of the T1w and T2-FLAIR images in the FreeSurfer processing (Lindroth et al. 2019). We observed some variability of the vertices' variance between samples, although concordance remained high (Figures S2–S5). This led us to flag 'noisy' vertices that exhibited outlying variance in at least one sample (> 6SD from the regression lines shown in Figures S2–S5), which could suggest they are prone to measurement error in some of the samples. About 1% of the vertices were flagged, equally distributed across each type of measurement (Figures S6 and S7, Table S2), although some brain regions contained a large proportion of flagged vertices (37% of anterior cingulate [thickness] consisted in flagged vertices, 35% of entorhinal gyrus [thickness], 18% of temporal pole [thickness], and 35% of the accumbens [surface area], Table S2). Considering the overall small number of 'noisy' vertices, we included them in the subsequent analyses, so we could evaluate if they were more likely to reach significance in association testing.

2.5 | Methods

We performed association testing within each discovery sample (Table 1) and meta-analysed the results. We used PISA and MEMENTO to replicate the significant associations and to test the out-of-sample prediction.

2.5.1 | Analyses Using Grey-Matter Regions of Interest (ROI)

First, we estimated the total association (ROI based morphometricity) between each of our traits of interest and the 150 ROI measurements of grey-matter structure (cortical thickness and surface area; subcortical volumes). We used multiple regression, using the lm() function in R (version 4.2.2), and compared the full model (ROI and covariates) to a 'null model' that only included covariates. We reported the difference in adjusted R^2 between the two models and estimated its standard error using bootstrap (*boot* package). Finally, we tested whether the ROI-based R^2 (ROI based morphometricity) was significantly different from zero using a likelihood ratio test (*lmtest* package). From the full model, we also extracted the conditional associations between the ROIs and the traits of interests. These associations correspond to that of each ROI, while controlling for covariates and all other ROIs. We can expect that these associations are free from redundant (or false positive) associations that arise from correlated ROI measurements.

Next, we estimated the ROI-traits associations using 150 different linear regressions (i.e., one regression per ROI) that control for covariates. Unlike for the conditional associations (from multiple regression), some of the univariate associations may be (in part, or fully) redundant, in that they would tag signal from correlated ROIs. We expect the association effect sizes to be larger and to be more often significant, compared to the model that fits all ROIs at once.

2.5.2 | Vertex-Wise Association Studies

We first used a General Linear Model (GLM), which has been more commonly used in mass-univariate association testing and can be written as:

$$\mathbf{y} = \mathbf{x_i} b_i + \mathbf{Zc} + \boldsymbol{\varepsilon} \quad (1)$$

where, $\boldsymbol{y}$ is a vector of size N of the trait of interest, $\mathbf{x_i}$ is a vector of the ith vertex-wise measurement and b_i the association effect size (between each vertex and the trait of interest) we seek to estimate. $\mathbf{Z}$ is a matrix of size Nxq of q covariates and $\mathbf{c}$ a vector of the q fixed effects. $\boldsymbol{\varepsilon}$ is the error term assumed to follow $\boldsymbol{\varepsilon} \sim \mathcal{N}\left(0, \mathbf{I}\sigma^2_{\boldsymbol{\varepsilon}}\right)$.

In addition, we used a linear mixed model (LMM), which is an extension of the GLM that further controls for all vertex-wise measurements, fitted as a random effect. We have shown using simulations that this approach could remove many redundant associations detected by the GLM, some of which are likely to be spurious associations caused by imaging confounders responsible for short and long-range correlations between brain measurements(Couvy-Duchesne, Zhang, et al. 2020; Couvy-Duchesne et al. 2021). The model becomes:

$$\mathbf{y} = \mathbf{x_i} b_i + \mathbf{Zc} + \mathbf{X}\boldsymbol{\beta} + \boldsymbol{\varepsilon} \quad (2)$$

With, $\mathbf{X}$ the Nxp matrix of all standardised vertex-wise measurements, and $\boldsymbol{\beta}$ a px1vector of random effect assumed to be normally distributed with variance $\sigma^2_{\boldsymbol{\beta}}$: $\boldsymbol{\beta} \sim \mathcal{N}\left(0, \mathbf{I}\sigma^2_{\boldsymbol{\beta}}\right)$. Fitting $\mathbf{X}\boldsymbol{\beta}$ as a random effect allows for the case where there are more vertex-wise measurements than individuals ($p > N$). The variance–covariance matrix for $\mathbf{Y}$ is $\mathrm{var}(\mathbf{Y}) = \mathbf{X}\mathbf{X}'\sigma^2_{\boldsymbol{\beta}} + \mathbf{I}\sigma^2_{\boldsymbol{\varepsilon}} = \mathbf{B}\,\mathrm{p}\sigma^2_{\boldsymbol{\beta}} + \mathbf{I}\sigma^2_{\boldsymbol{\varepsilon}}$. Here, we recognise $\mathbf{B} = \mathbf{X}\mathbf{X}'/\mathrm{p}$ as the brain relatedness matrix and $\mathrm{p}\sigma^2_{\boldsymbol{\beta}}$ the morphometricity (phenotypic variance captured by the total association with all vertices) (Couvy-Duchesne, Strike, et al. 2020).

In addition, we used a LMM in which we fitted cortical and subcortical measurements, as well as thickness and surface area as specific random effects. We found using simulations, that this model was best suited to the situation where some modalities are not associated with the trait of interest (Couvy-Duchesne, Zhang, et al. 2020). The model becomes:

$$\mathbf{y} = \mathbf{x_i} b_i + \mathbf{Zc} + \mathbf{X_1}\boldsymbol{\beta_1} + \mathbf{X_2}\boldsymbol{\beta_2} + \mathbf{X_3}\boldsymbol{\beta_3} + \mathbf{X_4}\boldsymbol{\beta_4} + \boldsymbol{\varepsilon} \quad (3)$$

$\mathbf{X_1}$, $\mathbf{X_2}$, $\mathbf{X_3}$, $\mathbf{X_4}$ are the matrices of standardised vertex-wise measurements from cortical thickness, cortical surface area, subcortical thickness and subcortical surface area. Each

$\boldsymbol{\beta}_j \sim \mathcal{N}\left(0, \mathbf{I}\sigma^2_{\boldsymbol{\beta}_j}\right)$ (j in 1–4) is the vector or vertex trait associations specific to each random effect. This means that each $\sigma^2_{\boldsymbol{\beta}_j}$ quantifies the trait variance that is accounted for by a set of measurements, which can be 0.

LMM and GLM models are implemented in the efficient OSCA software, which allows performs hundreds of thousands of tests in minutes using low memory (RAM) requirements (Zhang et al. 2019).

2.5.3 | Statistical Testing and Multiple Comparisons for Vertex-Wise Models

We performed a χ^2 test of the association between the phenotype and each vertex $(\mathbf{X_i})$ using that: $\left(\frac{b_i}{SE(b_i)}\right)^2 \sim \chi^2_1$ under the null hypothesis of no association. We corrected for multiple testing using Bonferroni correction, which allows to control false positive rate across several surfaces (left and right hemisphere, cortical thickness and area) and may be best suited to analyses on unsmoothed data (Nichols and Hayasaka 2003). We further corrected for the number of phenotypes tested (24, Table 1), which resulted in a significance threshold of 3.18e-9 for reporting significant vertex-wise associations.

Finally, we also applied Random Field Theory (RFT) as an alternative to Bonferroni, which models the spatial autocorrelations of the test statistics across a surface We applied a recent implementation of vertex-wise RFT from the NeuroShape toolbox (https://github.com/nikitas-k/neuroshape-dev/tree/main/neuroshape/) to our cortical and subcortical surfaces of interest: NeuroShape only requires, for each surface, the vertices coordinates and corresponding t-statistic of association. We used a significance threshold of 0.05/24/18 = 1.1e-4 to account for the number of grey-matter surfaces (18) and traits tested (24).

2.5.4 | Vertex-Wise Morphometricity

For each trait and each sample, we reported the vertex-wise morphometricity, which corresponds to the total association between the trait and all (vertex-wise) measurements(Couvy-Duchesne, Strike, et al. 2020; Sabuncu et al. 2016). In practice, morphometricity is expressed as a proportion of the trait variance (R^2) and estimated from a mixed model. It can estimated as $R^2 = \frac{\sigma^2_{\beta}}{\sigma^2_{\varepsilon}+\sigma^2_{\beta}}$ for model (2), or $\frac{\sigma^2_{\beta_1}+\sigma^2_{\beta_2}+\sigma^2_{\beta_3}+\sigma^2_{\beta_4}}{\sigma^2_{\varepsilon}+\sigma^2_{\beta_1}+\sigma^2_{\beta_2}+\sigma^2_{\beta_3}+\sigma^2_{\beta_4}}$ for model (3) (Couvy-Duchesne, Strike, et al. 2020). Model (3) also allows to decompose the morphometricity into the (joint) contributions of each type of measurement (e.g., $\frac{\sigma^2_{\beta_1}}{\sigma^2_{\varepsilon}+\sigma^2_{\beta_1}+\sigma^2_{\beta_2}+\sigma^2_{\beta_3}+\sigma^2_{\beta_4}}$ for the contribution of cortical thickness). The difference between vertex-based morphometricity and ROI based morphometricity indicates how much information may be lost by averaging brain measurements over ROIs, compared to using the full (vertex-wise) resolution.

2.5.5 | Covariates

We considered standard imaging covariates, that were available for all samples: age, sex, age^2, age × sex, intra-cranial volume (ICV, estimated from FreeSurfer 6.0), average cortical thickness and total cortical surface area (also estimated from FreeSurfer), site/scanner and field strength when pertinent (data sets AIBL, OASIS3). We did not consider the extended set of covariates that was recently suggested for the UKB (Alfaro-Almagro et al. 2021), as they were not available outside of the UKB (e.g., time since first scan, head-motion measured from resting-state fMRI). When studying neuropsychological scores, we further corrected for AD and MCI status, to be able to compare and meta-analyse results across cohorts that contain different proportion of cases and MCI (Table 1).

2.5.6 | Meta-Analysis

We meta-analysed the association maps from the discovery samples (ADNI1, ADNI2GO2, AIBL, ARWIBO, EPAD, MAS, OASIS3, OATS) using the Inverse Variance Weighted (IVW) approach, implemented in the R package *meta* (Balduzzi, Rücker, and Schwarzer 2019) (metagen function). We used a random effect approach, which considers that the different samples are randomly drawn from a global population. In particular, we used the REML method, which provides of the most robust estimates of the between-study variance (i.e., heterogeneity) (Veroniki et al. 2016), and we reported heterogeneity across studies using the Q statistic. Our meta-analytic approach is conservative, but also ensures the findings are generalisable in that only homogeneous association effect sizes across cohorts reach significance.

2.5.7 | Replication and Out-of-Sample Prediction

We used MEMENTO and PISA to evaluate the stability of the morphometricity estimates and the replicability of the significant brain-trait associations obtained from the meta-analyses. Using PISA, we could attempt to replicate results that involved AD cases, RAVLT scores. In MEMENTO, we sought to replicate the findings relating to AD conversion and all other neuropsychological scores (e.g., MMSE, CDR, FAQ, logical memory).

We used out-of-sample prediction (into MEMENTO and PISA) to compare and validate the findings from the ROI and vertex-wise association maps. Out-of-sample prediction gives confidence that the identified brain-trait associations are true and generalisable. It also quantifies the total association between a trait and all grey-matter markers identified in the analyses. We used prediction accuracy to compare results obtained using, ROI, GLM or LMM association models or using Bonferroni versus RFT to account for multiple testing.

The linear prediction scores were built using the weights from the meta-analysed association maps. For vertex-wise association maps, we only included the top vertex per cluster (i.e., vertex with the smallest pvalue), as we can assume that the other voxels of the cluster tag the same information. We used the Bonferroni significance level (3.18e-9) or RFT corrected p-value < 0.05 to define significant clusters. We reported the prediction accuracy as an R^2 (to facilitate comparison with morphometricity), which we estimated using a linear model that included the covariates.

2.5.8 | Cross-Trait Prediction

We evaluated how much the brain prediction scores could predict different—albeit related—phenotypes in MEMENTO and PISA. This design can help tackle specific research questions about disease subtypes and progression. For example, we evaluated the performance of Alzheimer's brain score to predict levels of amyloid beta and tau, which can inform on the relationship between grey-matter structure and protein concentration. We also investigated if the AD brain score could differentiate MCI from controls, predict AD conversion as well as cognition and functioning. These results can shed lights on whether the same brain regions contribute to disease symptoms, subtypes, progression, or severity. This cross-trait prediction (a.k.a. transfer learning) also leverages that the samples sizes are larger for AD versus controls than for conversion or some neuropsychological scores, which may produce a more performant predictor, even if the trait predicted differs from the one used in training.

3 | Results

3.1 | ROI Based and Vertex-Wise Morphometricity

We estimated the morphometricity R^2 which quantifies the global association between a trait and all grey-matter measurements. We contrasted the morphometricity (Figure 1) obtained from vertex-wise data (>654,000 measurements) from that obtained using a ROI representation of the grey-matter (150 measurements). The difference in morphometricity between vertex-wise and ROI analyses indicates how much information is lost when reducing the dimensionality of the brain (here by a factor 4300 [654,000/150]).

We found that most traits (19 out of 24) exhibited a significant morphometricity (Figure 1, darker colours indicate p-value $<0.05/24$; full details in Table S3–S5). Vertex-wise morphometricity was 3 to 21 times larger than the ROI based one (Figure 1). For example, it was 3.6 times larger for Alzheimer's case control ('AD versus HC'), 14 times larger for the MMSE and 20 times larger for the CDR or the FAQ. Vertex-wise morphometricity of Alzheimer's disease and conversion was large (100% of variance accounted for when considering global brain measurements and vertex-wise measurements, Figure 1), indicating that cases and converters may be completely distinguished from controls, based on their grey-matter structure. In comparison, the vertex-wise morphometricity of MCI was lower (AD versus MCI: $R^2=0.64$, SE=0.10; MCI versus HC: $R^2=0.68$, SE=0.11), and that of neuropsychological scales ranged between 0.52 (SE=0.069, FAQ) and 0.044 (SE=0.059, RAVLT forgetting). Interestingly, family history of Alzheimer's disease (whether maternal or paternal) did not exhibit a significant morphometricity, suggesting the total association is null or too small to be detected at the current power. Using the UK Biobank, we confirmed that morphometricity of parental history was low. Vertex-wise morphometricity of maternal AD was 0.022 (SE=0.0054, p-value=3.8e-5, N=37,374), and not significantly different from zero in paternal AD ($R^2=0.0021$, SE=0.0033, p-value=0.53, N=31,739).

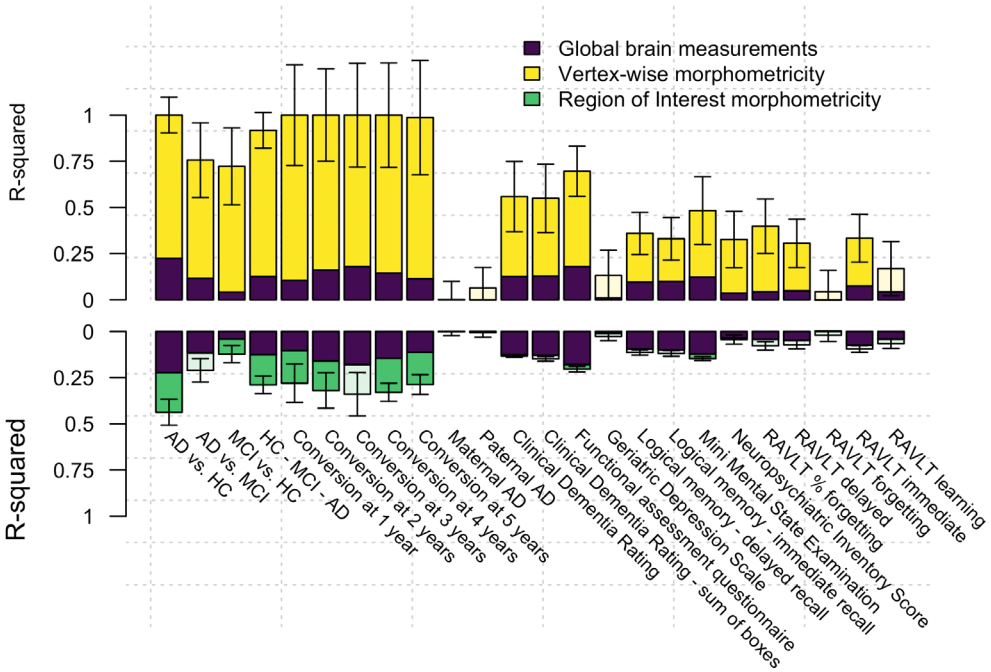

FIGURE 1 | Morphometricity from ROI and vertex-wise representation of grey-matter structure. Morphometricity from vertex-wise brain data (fitted as a single random effect) is shown in yellow in the upper bar plot, while the ROI based morphometricity is shown in green in the lower barplot. The trait variance accounted for by the global brain measurements (ICV, average cortical thickness and total cortical surface area for left and right hemisphere) is shown in purple. Whiskers represent the 95% confidence intervals around the morphometricity estimates. Bars with lighter yellow or green colours indicate morphometricity estimate not significant after multiple testing correction ($p>0.05/24$). For each bar, morphometricity (whether vertex or ROI based) as well as the R^2 accounted for by global brain measurement has been estimated in each clinical cohort and combined using a meta-analysis. Here, we report the morphometricity of neuropsychological scores (CDR, FAQ, GDS, LM, NPI and RAVLT) controlling for AD and MCI status.

The two vertex-wise models (i.e., fitting all measurements as a single random effect, or fitting them as 4 modality-specific random effects) yielded comparable morphometricity estimates (Figure S8). However, we can explore the contribution of each modality to the global morphometricity (by looking at the variance explained by each modality-specific random effect, Figure 2). The results indicate that cortical thickness significantly ($p < 0.05/24/4$) contributes to the morphometricity of Alzheimer's disease status, AD conversion, CDR, FAQ or the MMSE scores. In addition, we could confirm that subcortical thickness and surface area also significantly contribute to the morphometricity of Alzheimer's disease. Such analysis has a lower power, due to smaller association R^2 (compared to global morphometricity) and increased multiple testing, meaning that larger samples will be required to precisely estimate the contribution of each type of measurement to the global morphometricity.

The vertex-wise morphometricity we presented in Figure 1 was meta-analysed across all the discovery samples, and we note that the estimates appeared consistent across the different cohorts, as shown in the forest plots, and estimates of between-sample heterogeneity (Figures S9 and S10). The exception was for the MMSE and CDR scores, that showed a heterogeneous morphometricity across samples, even when controlling for disease and MCI status (Figure S10, $I^2 = 74\%$, Q-test, p-value $< 0.05/24$). However, the heterogeneity was greatly reduced ($I^2 = 51\%$ and $I^2 = 23\%$, p-value > 0.05) when estimating the morphometricity with modality-specific random effects (Figure S11), even if the meta-analysed result remained the same. This confirms the results from our simulations that a model with several variance components is more robust at estimating morphometricity, as it allows the different types of measurements to contribute more or less to the morphometricity (Couvy-Duchesne et al. 2022; Couvy-Duchesne, Zhang, et al. 2020). Finally, we observed that controlling for disease status, when studying neuropsychological scores reduced the between-cohort heterogeneity of results, as the morphometricity was inflated in the cohorts that contained Alzheimer's cases (Figure S12).

3.2 | Associations With Global Brain Measurements

We tested the associations between global brain measurements (ICV, left and right cortical thickness and left and right cortical surface area, fitted together in a multiple regression) and our phenotypes of interest, to shed light on the ones contributing to the variance explained reported in Figures 1 and 2. We controlled for all other covariates in the linear models and meta-analysed the results across samples. Larger ICV was associated with Alzheimer's disease, Alzheimer's conversion (at 3, 4 and 5 years) and with FAQ score. In addition, Alzheimer's cases also exhibited thinner left and right cortex, compared to controls. Individuals who converted within 4 years of brain imaging had a thinner left cortex. Finally, greater MMSE and RAVLT immediate memory scores were associated with thicker left cortex, and MMSE was further associated with larger left cortical surface area (Table S6).

3.3 | ROI-Based Associations

We sought to identify ROI measurements that contribute to the ROI based morphometricity reported in Figure 1. First, we focussed on the marginal associations between ROI and traits of interest, which are estimated using multiple regression where all 150 ROI measurements are fitted in a linear model, together with the covariates. Of note, these same models are used in Figure 1 to estimate ROI-based morphometricity. A single association survived multiple testing correction (p-value $< 0.05/24/150$), which suggested that hippocampal volume was associated with RAVLT delayed recall score. An increase of one SD in hippocampal volume was associated with a 0.79-point score increase (SE = 0.17, p-value = 3.3e-6, see Figure S13 for forest plot).

Next, we tested the association between traits and each ROI measurement, by including a single ROI in the linear model, and controlling for covariates. This is the standard approach in neuroimaging, for example used in the publications from the ENIGMA consortium (Thompson et al. 2020), although we can expect some redundancy in the identified associations. This time, we identified 94 trait-ROI associations after controlling for multiple testing (p-value $< 0.05/24/150$, Table S7). Left hippocampus volume was still associated with RAVL delayed recall score ($b = 0.79$-point increase per volume SD, SE = 0.11, p-value = 9.6e-14, Figure S13), but so were right hippocampus ($b = 0.62$) and right or left amygdala volumes ($b = 0.49$ and $b = 0.52$). Unlike in the multiple regression approach, the comparison of Alzheimer's versus healthy controls yielded 32 significant associations (Figure 3), which include smaller hippocampus and amygdala (to a lesser extend smaller putamen and accumbens), and reduced temporal lobe (fusiform, middle temporal, inferior temporal, parahippocampal gyri, temporal pole). In addition, we also identified larger cortical thickness or surface areas in the paracentral, precentral, and postcentral gyri, as well as in the pars-opercularis and superior frontal regions (Figure 3).

Alzheimer's disease conversion was associated with thicker lateral occipital gyrus, as well as thinner hippocampus, middle temporal, and fusiform gyri (Figure S14, Table S6). Logical memory scores measure how much participants can recall a story. Lower immediate and delayed recall were associated with smaller hippocampus and thinner entorhinal gyrus, as well as an increased precentral gyrus. However, immediate recall was further associated with pars triangularis, while delayed recall was associated with the amygdala and the parahippocampal gyrus (Figure S15). The RAVLT memory scores, that evaluate how many words of a list can be remembered, only implicated the hippocampus, amygdala, and the entorhinal cortex (for immediate recall) (Figure S15).

Lastly, the CDR, FAQ and MMSE were significantly associated with ROIs, mostly found to be associated with Alzheimer's disease, even if we controlled for disease status in the analyses (Figure S16). Associations were found with the hippocampus (MMSE), amygdala (MMSE, FAQ), middle temporal (CDR, MMSE), entorhinal (FAQ), inferior temporal (FAQ), postcentral (MMSE) as well as with the inferior parietal gyrus (MMSE).

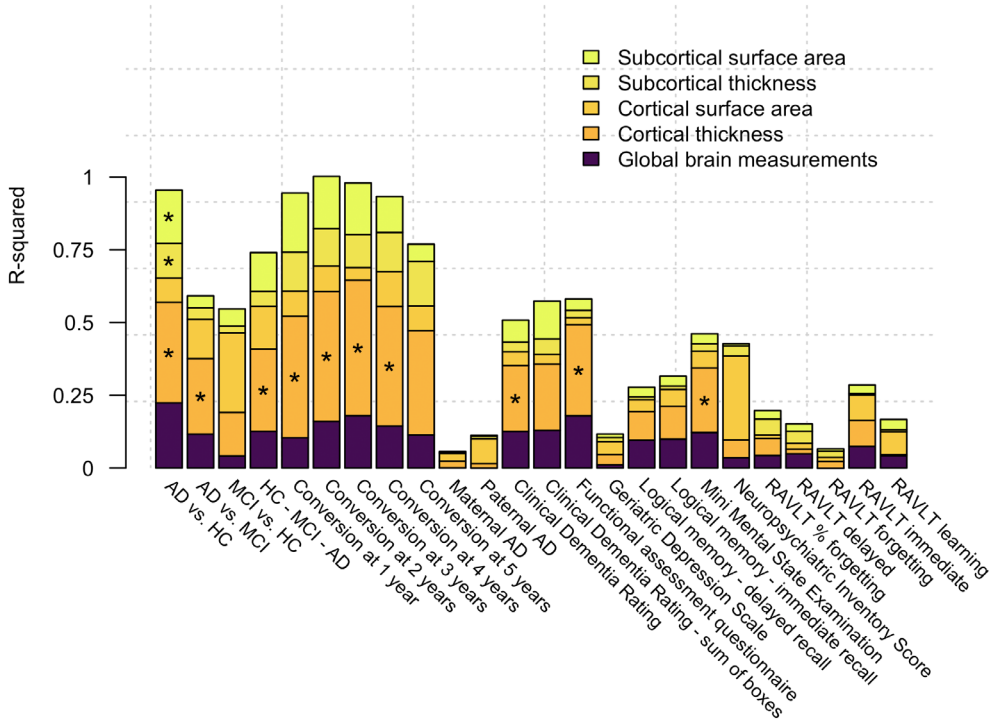

FIGURE 2 | Vertex-wise morphometricity broken down into the contributions of each modality of brain measurement. Contributions from the different modalities are estimated jointly by fitting each type of measurement as a specific random effect in a mixed model. Significant contributions, after multiple testing correction ($p < 0.05/24/4$) are highlighted by a star.

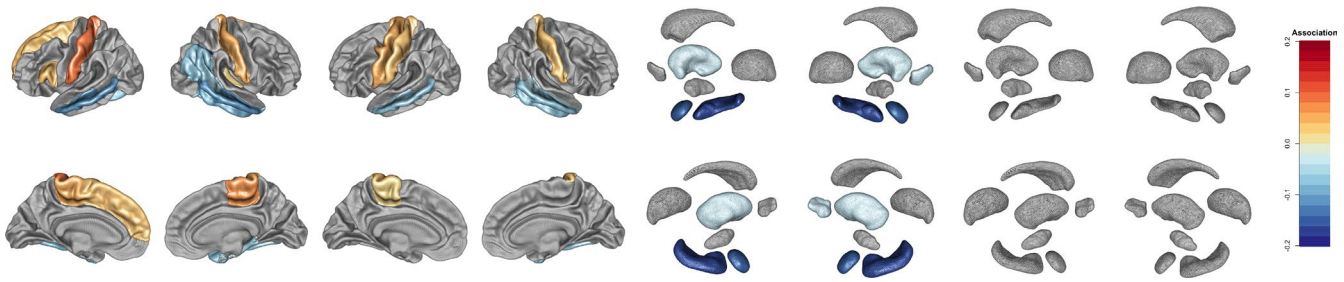

FIGURE 3 | Univariate ROI associations with Alzheimer's disease (Alzheimer's vs. healthy controls). Outside view (top panels) and Inside view (bottom panels). From left to right: Left cortical thickness, right cortical thickness, left cortical surface, right cortical surface, left subcortical volumes and right subcortical volumes. We only show significant ROIs after multiple testing correction ($p < 0.05/24/150$). The association effect sizes correspond to the effect of 1 SD of ROI on the clinical status (0: Controls, 1: Alzheimer's).

3.4 | Vertex-Based Associations

We performed vertex-based association testing, to identify the localised grey-matter regions that contribute to the vertex-wise morphometricity. As in the ROI based association testing, we performed traditional mass-univariate testing (i.e., testing the trait association with a single vertex: GLM model) as well as multi-vertex testing (i.e., estimating the trait-vertex association controlling for all other vertices: LMM model). We expect the GLM to yield more associations, although some would be redundant or confounded as they tag signal from other regions, whose association spreads though the brain connectome.

Using Bonferroni correction ($p < 3.1e\text{-}9$), the mass-univariate testing identified significant vertices for 16 (out of 24) traits (307 significant clusters overall). In comparison, the LMM with a single random effect, identified significant vertices for only 3 traits (AD versus HC, conversion at 2 and 3 years; 34 significant clusters in total) while the LMM with four random effects only found associations with AD versus HC (1 cluster; Figure S17, Table S8). Thus, when comparing Alzheimer's versus healthy controls, the mass univariate model returned 103 significant clusters (5523 significant vertex-wise measurements), that indicated smaller (thickness and surface area) bilateral hippocampus, amygdala, putamen and accumbens, as well as thinner pallidum (left and right), caudate (left) and lower surface of right thalamus. In addition, we observed thinner cortex in the temporal lobe (entorhinal, fusiform, parahippocampal, superior and middle temporal gyri, temporal pole) as well as associations in the insula, posterior cingulate, paracentral and precuneus (Table S9, Figure 4a, also see Figure S18 for unthresholded map). In comparison, the multi-vertex approach (LMM with a

single random effect) located the significant associations in the hippocampus and amygdala (lower thickness and surface area), and only implicated the right entorhinal and insula thickness, in the cortex (Table S10, Figure 4b).

Compared to MCI, Alzheimer's cases exhibited thinner left hippocampus and bi-lateral amygdala. The surface of the left hippocampus and right amygdala was also found to be smaller (GLM only; Table S9). Alzheimer's conversion was associated with smaller hippocampus and amydgala (using GLM and LMM), although the GLM identified many more significant clusters within those subcortical structures (Tables S9 and S10). In addition, the GLM identified clusters in the left temporal pole and right entorhinal that were thinner in converters than non-converters. Finally, most of the grey-matter regions associated with the neuropsychological scales (FAQ, LM-delayed, MMSE, RAVLT) were in the hippocampus (Table S9). The remaining significant clusters implicated the putamen, amygdala, and entorhinal gyrus (Table S9).

Nine clusters identified with GLM (2.9% of clusters), and three clusters found with LMM (8.8% of clusters) contained 'noisy vertices' (Tables S9 and S10) which we defined as having variable variance across samples. Compared to the overall proportion of 'noisy vertices' (1.1%) this suggests they are more likely to reach significance in the analyses. We also found that RFT to be more conservative that Bonferroni's correction for multiple testing (Table S8). Overall, RFT halved the number of significant clusters (120 versus 307 using GLM, 12 versus 34 using LMM, Table S8). The RFT significance threshold was specific to each cortical or subcortical surface. The most lenient RFT threshold was for the Accumbens (p-value < 2.9e-11) while the most stringent was for cortical thickness (p-value < 7.7e-16).

3.5 | Comparison of ROI and Vertex-Wise Associations

We represented (Figure 5) how much the significant ROIs co-localised with clusters found in the mass-univariate vertex-wise analysis (GLM), and with those found in the multi-vertex one (LMM). We focussed on AD versus HC, which yielded significant associations in 38 grey-matter regions, across the three approaches. Overall, only four (4/38 = 10%) grey-matter regions (left and right amygdala and hippocampus) were consistently identified across the three analyses. Nine additional grey-matter regions (cortical and subcortical) reached significant in the ROI-based and GLM vertex-wise analysis, and two were identified in both GLM and LMM analyses. Thus, only 15 (39%) of the identified grey-matter regions were significant in at least two analyses (Figure 5).

The concordance presented in Figure 5 does not take show whether the association was found with volume, thickness, or surface area, see detailed Sankey plots for all details (Figure S19). Furthermore, several clusters identified using GLM and LMM did not overlap, despite being located in the same grey-matter regions (e.g., hippocampus, Figure S19).

The analyses of Alzheimer's conversion consistently implicated the hippocampus (Figure S20), and the GLM and LMM identified clusters in the amygdala that were not detected in the ROI based analysis. Only one of the three LMM-identified cluster (in right amygdala thickness) partially overlapped with a GLM cluster (Figure S20).

Similarly, we observed mixed concordance for the ROI and GLM findings for the neuropsychological scales (Figures 21–25).

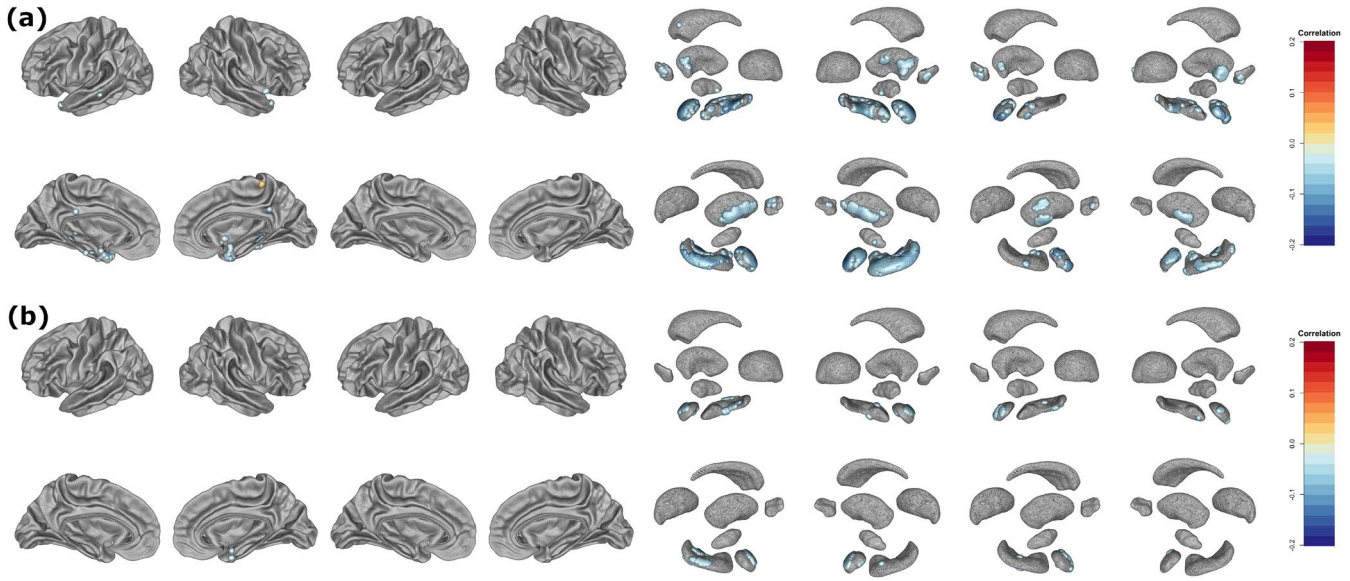

FIGURE 4 | Vertex-wise associations with Alzheimer's disease (Alzheimer's versus healthy controls). (a) mass-univariate (GLM) model, where the association with each vertex-wise measurement is estimated separately. (b) multi-vertex (LMM) model with a single random effect, where the association with each vertex-wise measurement is estimated conditional on all vertices fitted as a random effect. Outside view (top panels) and Inside view (bottom panels). From left to right: Left cortical thickness, right cortical thickness, left cortical surface, right cortical surface, left subcortical volumes and right subcortical volumes. We only show in colour the significant vertex-wise measurement after multiple testing correction ($p < 0.05/24/150$). The association effect sizes correspond to cohen's d, that is, the effect of 1 SD of the vertex measurements on the clinical status (0: Controls, 1: Alzheimer's).

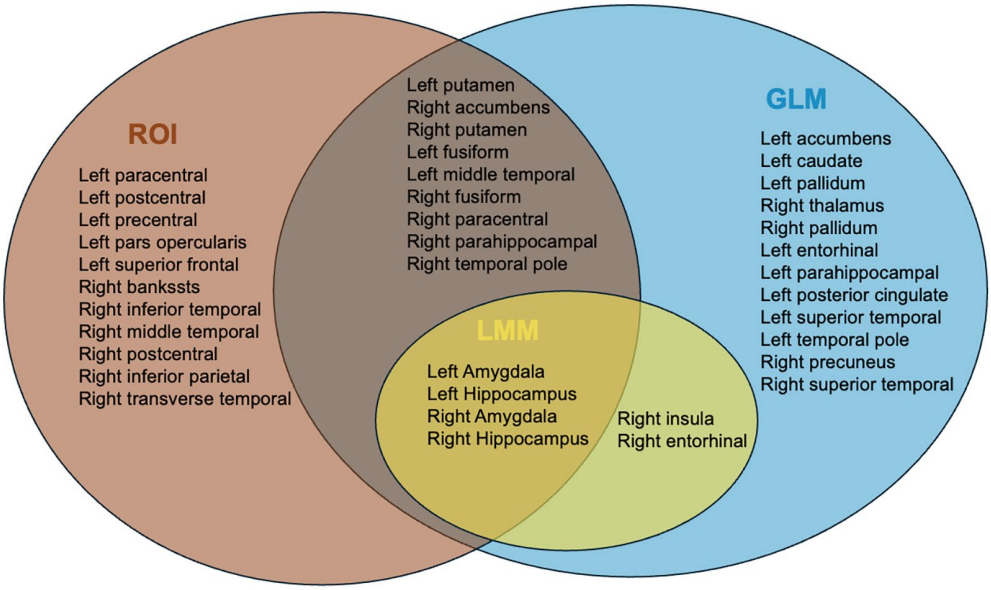

FIGURE 5 | Concordance of brain regions associated with Alzheimer's disease (AD versus HC) across the different analyses (ROI and vertex-wise [LMM or GLM]).

Comparison was not possible with the LMM due to the lack of significant clusters with this approach.

3.6 | Grey-Matter Regions Associated With Several Traits

The large number of significant clusters found in the subcortical volumes (in particular the hippocampus and amygdala) led us to investigate whether the same vertices/clusters were associated with several traits.

We found a substantial overlap between the vertex-wise measurements associated (using GLM) with the different traits of interest (Figure 6). For example, 92% of the associations with AD versus MCI were also found in the AD versus HC analysis, 54% of the associations with conversion at 2 years were also found when studying conversion at 3 years, and 74% of the measurements associated with conversion at 4 were also found for conversion at 5 years. However, conversion at 2 or 3 years seemed to implicate different brain regions than conversion at 4 or 5 years (only 3%–4% overlap, but still greater than what may be expected by chance). In addition, a significant fraction of the vertex-wise measurements associated with neuropsychological scales were also significance in AD versus HC, despite controlling for disease status in the analyses. The overlap was particularly important with the FAQ (88% of the 57 associations also significant in AD versus HC), or the MMSE (18 out of 20 associations (90%) significant in AD versus HC). Lastly, we observed significant overlap between the brain feature associated with the different memory scores (between RAVLT sub-scores and between RAVLT and Logical Memory score).

Some brain regions in the hippocampus and amygdala, were significantly associated with up to 6 distinct traits (Figure S26, Table S11), and may be of particular interest as they could point out to key brain regions associated with Alzheimer's, functioning and cognition. For example, a smaller surface of left hippocampus (around vertex 776) was associated with increased conversion at 3 years and lower memory scores (RAVLT—delayed, immediate, learning and forgetting, as well as Logical memory delayed recall). In addition, thinner right amygdala (around vertex 1133) was associated with increased risk of Alzheimer's (AD versus HC and AD versus MCI), lower functioning (FAQ) and memory (RAVLT delayed and immediate).

3.7 | Replication of Associations

We found consistent vertex-based morphometricity estimates in the PISA and MEMENTO replication samples, compared to those from the meta-analysis (correlation between discovery and replication estimates 0.76 in PISA, 0.74 in MEMENTO, Figure S27). The largest discrepancies were found for MCI versus HC, conversion at 1 year, and CDR score, which exhibited a lower morphometricity in MEMENTO than in the meta-analysis, although this may be due to sample composition and recruitment (HC of MEMENTO all have subjective cognitive decline). Concordance was also observed for ROI based morphometricity (correlation between discovery and estimates: 0.80 in PISA, 0.84 in MEMENTO, Figure S28).

We sought to replicate the 94 ROI associations that were significant in the meta-analysis of clinical cohorts (Table S7). In PISA, we evaluated 57 associations (based on the phenotypes being available), and 12 reached significance (p-value $< 0.05/57$); 28 were nominally significant (p-value < 0.05). Beyond significance, we found good concordance of the effect sizes between discovery and replication (cor $= 0.92$ between effect size, 90% had the same sign). The 12 associations that replicated corresponded to reduced cortical thickness in Alzheimer's (left middle temporal gyrus, right posterior banks of the superior temporal sulcus, right inferior parietal, right inferior temporal, right, paracentral, and right postcentral), as well

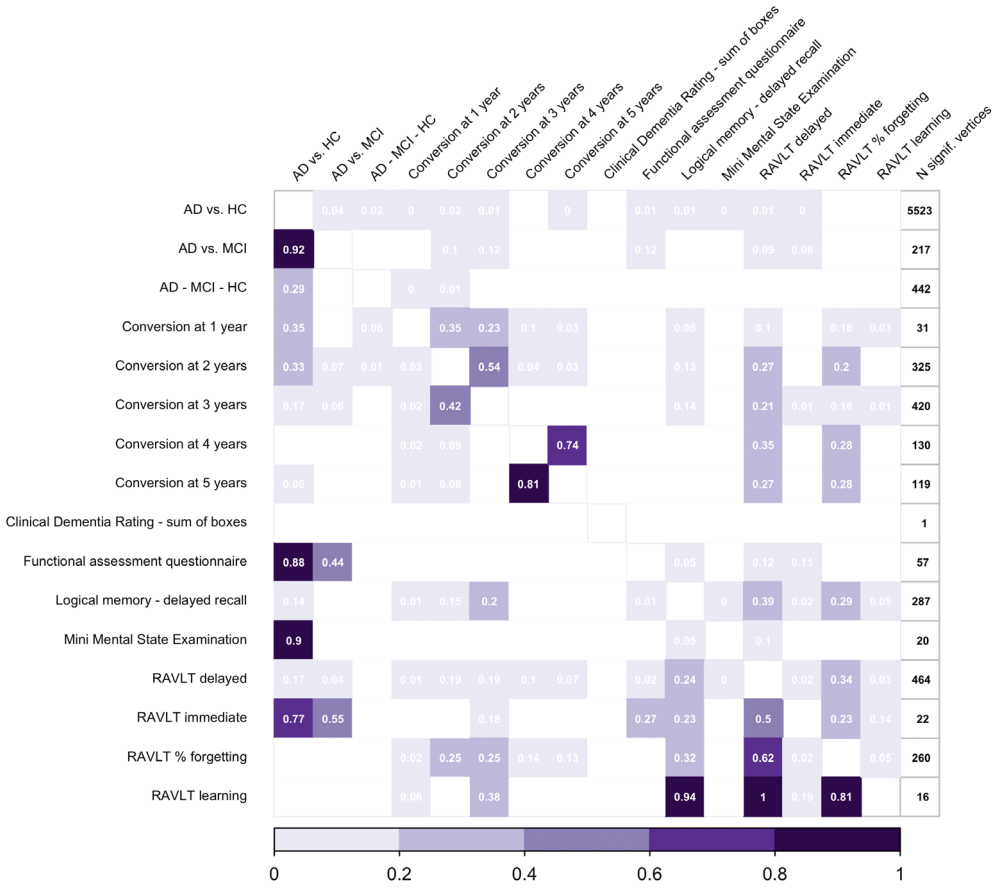

FIGURE 6 | Proportion of significant vertex-wise measurements (from GLM) also associated with another trait. Each cell indicates the proportion of vertex-wise measurement associated with a phenotype (row label), that is also significantly associated with another phenotype (column label). For example: 92% of the vertex-wise measurements associated with AD versus MCI are also associated with AD versus HC (first column, second row). We only show cells for which the proportion of co-associated vertices was greater than chance (chi-2 test of association, p-value < 0.05/(24*23/2)). Significant vertex-wise measurements correspond to those that pass Bonferroni correction using the mass-univariate (GLM) approach. Traits with no significant vertex-wise measurements are not shown. The last column shows the number of significant vertex-wise measurement, for context.

as reduced volumes of hippocampus and amygdala. In addition, we also replicated the positive associations between bilateral hippocampal volume and RAVLT delayed memory score (Table S7). In MEMENTO, we evaluated the other 37 associations, and 9 reached significance (p-value < 0.05/37; 19 nominally significant, cor = 0.71 between discovery and replication effect sizes, 81% of sign concordance). The replicated associations confirmed lower hippocampus volume and middle temporal thickness in AD converters (3 years conversion). In addition, logical memory scores (immediate and delayed) were associated with hippocampal, and amygdala volumes, as well as with entorhinal thickness (Table S7).

At a vertex-wise level using the GLM approach, we replicated one association in PISA (left-putamen surface area association with AD; p-value < 0.05/183), although 41 (22%) of the tested vertices were nominally significant in the replication sample suggesting an enrichment, despite a low sample size and statistical power. In MEMENTO, we replicated 65 (54%) associations (p-value < 0.05/120), and 83% were nominally significant. The replicated associations were with logical memory delayed recall score (entorhinal, hippocampus and amygdala) as well as with Alzheimer's conversion (bilateral hippocampus, amygdala, and right entorhinal gyrus) (Table S9). As per the LMM results, we replicated 6 (out of 30%–20%) associations with AD versus HC in PISA (p-value < 0.05/30), that corresponded smaller surface area in bilateral hippocampus and left amygdala, as well as reduced thickness in left hippocampus and right amygdala. In total, 17 (57%) of the associations were nominally significant in PISA, and all signs were concordant between discovery and replication effect sizes. In addition, we replicated 1 (out of 4) association with AD conversion at 3 years, located in the right amygdala (thickness).

3.8 | Out-of-Sample Prediction

To validate but also to compare the different set of results obtained in ROI or vertex-based analyses, we evaluated their prediction accuracy in the PISA and MEMENTO cohorts.

In PISA, we found that the three analyses (ROI, GLM, LMM) led to a prediction of Alzheimer's status (versus controls), significantly greater than chance. Prediction accuracy was comparable across the three predictors as indicated by overlapping confidence intervals: $R^2_{ROI} = 0.12$ (95% CI 0.05–0.19, p-value = 3.5e-12), $R^2_{GLM} = 0.07$, (95% CI 0.01–0.15, p-value = 4.6e-7) and $R^2_{LMM} = 0.13$, (95% CI

0.05–0.22, p-value = 6.2e-13, which corresponds to OR = 4.1 or AUC = 0.71) (Table S12). We also found that the ROI or vertices associated (via GLM) with RAVLT scores had significant predictive power in PISA, although prediction accuracy was limited ($R^2 < 0.035$, Table S12).

In MEMENTO, the significant brain measurements could significantly predict AD conversion, although the best predictor was $R^2_{GLM} = 0.051$ (equivalent to AUC = 0.63), for AD conversion at 3 years (p-value = 1.6e-21). Overall, the ROI and vertex-wise approaches led to comparable prediction (Table S12). In addition, we also observed significant prediction accuracy from the MMSE and logical memory (immediate recall) brain markers ($R^2 < 0.014$).

In addition, we found that the AD versus HC predictors could predict several traits and scores in the PISA or MEMENTO non-diseased (HC + MCI) group. In PISA, the AD brain risk scores were associated with MCI status, presence of memory and language impairment, as well as the number of impaired cognitive processes. Furthermore, the brain risk scores could predict some of the cognition scores (Graded Naming Test, and RAVLT scores), as well as the individuals' genetic risk (Figure 7, Table S13). In MEMENTO, the AD versus HC predictors could significantly predict multi-domain amnestic MCI status, AD conversion (at all time frames), a series of neuropsychological scores (MMSE, CDR, naming test, visual memory), as well as *APOE e4* status and total Tau protein level, measured from lumbar punction (Figure 7, Table S13). The AD brain scores achieved comparable prediction accuracy ($R^2 < 0.06$) as the specific predictors of AD conversion or neuropsychological scores (MMSE, CDR) (Table S12).

4 | Discussion

We collated data from 10 cohorts (total $N = 9140$) to perform a well-powered Brain Wide Association Study of the grey-matter structure in Alzheimer's disease, progression to AD, and neuropsychological scores. The large sample size and deep clinical characterisation supported identification of identified grey-matter markers associated with the different stages of the disease: early disease risk (markers of conversion up to 5 years prior to diagnosis), non-specific first symptoms (mild cognitive impairment), specific memory and functioning complaints, as well as (post-)diagnostic markers (Figures 3 and 4) that may be indicative of disease progression and severity. Our results suggest some overlap between the grey-matter regions associated with early (pre-diagnostic) AD risk, disease progression and memory domains (Figure 6, Table S11), which progresses our understanding of the clinical correlates of grey-matter atrophy and allows cross-trait prediction. Thus, we showed that brain markers associated with disease status could predict global tau pathology, AD genetic risk (measured from SNPs), progression to dementia, and cognitive domains in non-diseased individuals (Figure 7). Our results are robust and generalisable to other cohorts or studies, as shown by the high replication rate (Tables S7 and S9) and out-of-sample prediction accuracy (Table S12). Another strength of our study is that we performed multi-level brain analyses, that is, at a region of interest but also at the vertex-wise level. The high-resolution (vertex-wise level) analysis increased the characterisation of some of the associated brain regions, but also identified of novel brain regions that could not be detected using the traditional ROI approach (Figure 5).

4.1 | Medial Temporal Lobe in Alzheimer's' Disease

The comparison of AD cases versus healthy controls, yielded the most associations, either at the ROI or vertex-wise level (Figures 3 and 4). Our ROI-level results confirmed the known atrophy of hippocampus volume (cohen's $d = -0.17$), amygdala volume ($d = -0.15$) and of the medial temporal lobe (e.g., reduced thickness in fusiform [$d = -0.08$] and parahippocampal gyrus [$d = -0.05$]) (Table S7), which are known to play an important role in memory processing (Raslau et al. 2015). Previous publications (Frisoni et al. 2008; Schuff et al. 2009; Vijayakumar and Vijayakumar 2012) have reported somewhat larger hippocampal reductions in AD (equivalent to cohen's d in −0.26 −0.36, Appendix B), although we can expect their results to be inflated by winner's curse due to small sample sizes (Marek et al. 2022), the inclusions of more severe cases, or unaccounted sex and age differences between cases and controls (Appendix B). Overall the effect sizes we observed in the ROI-based analysis are comparable to the ones reported by the ENIGMA consortium on Parkinson's disease (Laansma et al. 2021), and for most psychiatric disorders (Thompson et al. 2020). All the ROI level associations (in subcortical and medial temporal cortex) were matched by one or several significant clusters in the vertex-wise analysis (Tables S9 and S10, Figures 5 and S19) which offers a more fined grained localisation of the grey-matter associations. We confirmed these brain regions (ROIs) to be implicated in memory processes, as indicated by their association with episodic memory (RAVLT and logical memory scores, Table S7, even after controlling for disease status). Importantly, the entorhinal cortex, often reported to be an early site of atrophy (Johnson et al. 2012), was not significant in the ROI analysis, but several atrophied clusters were found at the vertex-wise level (Figures 5 and S19, Tables S9 and S10), which highlights the added value of high-resolution analyses. The vertex-wise analysis further pinpointed localised regions in the amygdala and hippocampus that were simultaneously associated with AD status and episodic memory scores (Table S11). Furthermore, reduced thickness and surface area in parts of the hippocampus and amygdala was observed several years prior to the diagnosis (see Table S11 for the list of vertex-wise markers of AD versus HC also associated with AD conversion, Figures S14 and S20), which confirms that the atrophy appears in early stages of the disease process (Johnson et al. 2012). Lastly, the vertex-wise associations we observed in the hippocampus (Figure 4) resemble that reported in a previous article (see Figure 5 from Frisoni et al. 2008) that reported smaller regional volume in the dorsal (CA1) and ventral parts (subiculum and presubiculum).

4.2 | Associations Between AD and Other Cortical and Subcortical Regions

We found associations between AD status and the putamen (ROI volume: $d = -0.04$, and vertex-wise clusters), or the accumbens

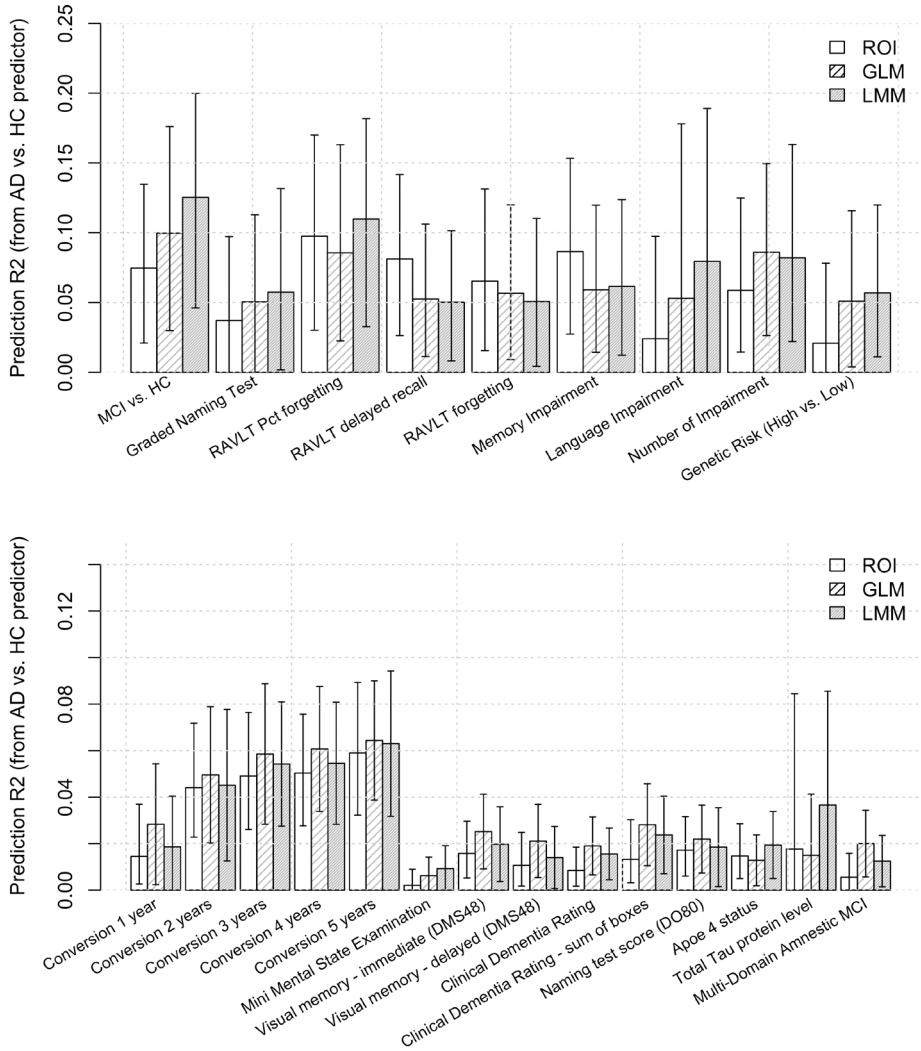

FIGURE 7 | Prediction accuracy of the AD versus HC brain predictors in the non-diseased group of the PISA and MEMENTO study. In PISA (top panel) evaluated prediction across 33 traits or scores available in the non-diseased group, and we show the nine for which at least one of the brain-based prediction returned significant ($p < 0.05/33/3$). In MEMENTO (bottom panel), we considered 36 traits, and 14 were significantly predicted ($p < 0.05/36/3$) by at least one of the AD versus HC brain predictor. Error bars correspond to the 95% confidence intervals estimated via bootstrap.

(ROI volume, $d = -0.03$) (Figures 3 and 4), which have been previously reported in smaller studies (de Jong et al. 2008, 2012). In addition, atrophy of the basal nuclei in Alzheimer's is thought to relate to general cognitive dysfunction (de Jong et al. 2008), and apathy (Guo et al. 2022). Coherent with this hypothesis, we found locally reduced right and left putamen thickness, associated with AD status as well as with impaired functioning (Functional Assessment Questionnaire, Table S11). However, we did not replicate the published association with thalamus volume (de Jong et al. 2008).

In the cortex, we identified additional regions (ROIs only) associated with Alzheimer's disease (Figure 3, Table S7), including several (with inferior parietal, postcentral [parietal], middle temporal, transverse temporal, inferior temporal [temporal], paracentral, superior frontal [frontal]) that replicated in an independent cohort (PISA), which gives confidence in the findings. A previous review has suggested that the medial and posterior parts of the parietal lobe would be preferentially affected in early stages of AD (Jacobs et al. 2012), which does not align with our results based on a much larger sample size. Our findings in the frontal and temporal lobes might reflect disease progression and general decay in cognition and functioning, that these regions encode (Johnson et al. 2012), which was corroborated by associations of the same ROI with MMSE and CDR scores (Table S7). Although, we cannot rule out that some of these findings could be caused by some misdiagnosis of frontotemporal dementia or vascular pathology, as screening is not systematic across the cohorts, and differential diagnostic can be difficult at the early stage of the diseases. Surprisingly, we did not find an association between Alzheimer's disease and posterior cingulate structure (either at a ROI or vertex-wise level), a region known to display strong hypometabolic (PET) changes in early stages of AD (Minoshima, Foster, and Kuhl 1994; Brun and Gustafson 1976). Reduced thickness in posterior cingulate has been reported before (Choo et al. 2010; Lehmann et al. 2010; Lerch et al. 2005), but in small studies prone to false positive and inflated association estimates (Marek et al. 2022). More work is needed to clarify the link between posterior cingulate hypometabolism and grey-matter structure, which may only appear in later stages of Alzheimer's disease.

Overall, inconsistent results in the literature can come from the use of different cortical atlas, which can capture different (non-overlapping) information (Fürtjes et al. 2023). In addition, some of the ROI associations we have identified may be (partly) redundant with those observed with the medial temporal lobe due to the correlation between ROI measurements. Our attempt to estimate the specific ROIs-trait association appeared underpowered (no association reached significance), but may be investigated in larger samples, or in post hoc analyses.

4.3 | Grey-Matter Markers of Alzheimer's Conversion and Neuropsychological Scores

We also identified brain markers of AD conversion, beyond those also associated with Alzheimer's status. They included thicker lateral occipital cortex and larger cortical area of the middle temporal gyrus (Table S7), which replicated in the MEMENTO cohort. These brain markers could be specific to early stages of the disease, and have previously been implicated in object recognition (Grill-Spector, Kourtzi, and Kanwisher 2001), but also in face and emotion recognition, as well as reading ability (Tanaka 2001). Future studies should clarify if these regions remains associated in later stages of AD (e.g., at a vertex-wise level), or if these brain markers are stage specific. Together, the identified markers of AD conversion, could significantly predict an individuals' risk of receiving a diagnosis within 5 years of the brain MRI, in an independent sample (MEMENTO, Table S12). Prediction accuracy remained modest ($R^2 < 0.051$, i.e., AUC < 0.63, or cohen's $d < 0.46$) and below some of the published results (mean AUC = 0.74, range 0.59–100; across 48 studies). However, our predictors only include ROIs or vertex-wise measurements that reached significance and were not designed to maximise prediction accuracy. In addition, the accuracy previously reported is likely optimistic (or overfitted) as predictors were trained and evaluated on ADNI only (Ansart et al. 2021).

The brain markers associated with neuropsychological scores (after controlling for AD status) shed light on the grey-matter circuits associated with cognition domains and functioning. Currently, the identified brain regions largely overlapped with those found to be associated with AD (Figure 6), although larger imaging samples should reveal many more relevant (and specific) grey-matter regions, as indicated by the gap between morphometricity (Figure 1) and the variance currently explained by the identified regions (see prediction R^2, Table S12).

4.4 | Alzheimer's Brain Score Captures Disease Risk in Healthy Individuals

The overlapping patterns of association we observed between AD and neuropsychological scores (Figure 5) led to performant cross-trait prediction, in non-diseased individuals (Figure 7, Table S13). Thus, we found that AD brain scores were associated with MCI status (memory and language impairments), AD conversion, AD genetic risk (incl., APOE e4), total Tau level from cerebral spinal fluid (associations with phosphorylated Tau or Amyloid-beta did not reach significance), and a wide range of cognitive scores (Figure 7, Table S13), which can shed light on the nature of the AD-related grey-matter markers reported above. The robust and transferrable prediction accuracy (across traits and samples) suggests that our AD brain scores could be used widely, when samples sizes are too small to derive efficient predictors of related traits, or when AD status is not collected or available. For example, our AD brain score could (partly) differentiate MCI from HC in PISA (Figure 7, Table S13), while the direct analysis of MCI versus HC did not yield significant prediction accuracy (Table S12). In addition, the fact that similar grey-matter regions are associated with AD and related traits warrants the use of multivariate approaches, that could boost discovery in future studies.

4.5 | More Precise Grey-Matter Maps Require Larger Samples

Our analysis of almost 10,000 brain MRI has identified many associations between grey-matter and our traits of interests (94 significant ROIs, 307 clusters of significant vertices, across the 24 traits considered). However, our findings fail to account for the full morphometricity (either ROI based or vertex-based, Figures 1 and 2), suggesting that larger samples are needed to identify additional brain regions with smaller effects, or to estimate more precisely the association effect sizes. For example, the significant ROI associated with AD could explain 12% (SE = 3.6%) of the variance in case control status in PISA (Table S12), while we estimated a ROI based morphometricity of 21% (SE = 3.6%, Figure 1, Table S4) across the discovery samples ($R^2 = 27\%$, SE = 7.7% in PISA). Even more strikingly, the significant vertex-wise measurements accounted for 13% (SE = 4.4%, Table S12) of AD variance, well short of the vertex-wise morphometricity of 100% (SE = 6.4%, Figure 1, Table S5).

4.6 | ROI Versus Vertex-Wise Analyses

We conducted analyses on two scales ROI-wise and vertex-wise. Vertex-wise analyses allows detection of more localised associations at the cost of a higher multiple testing burden. For example, some of the ROI detected as significant (e.g., in the frontal regions, Figure 5), did not generate significant vertex-wise associations within the matched regions. However, we found 94 significant ROI associations (Table S7) but 307 clusters of significant vertices (Figure 4, Table S9), which indicates that vertex-wise analysis are also well powered using our current sample size. The different number of findings can be explained by the fact that vertex-wise analyses allow the detection of several, independent clusters of significant vertices within a ROI (e.g., Figure S19). For example, when using LMM that limit the detection of redundant associations (Couvy-Duchesne et al. 2022), we identified 9 significant clusters associated with AD in the left hippocampus. This exemplifies the fact that a lot of the brain variation is lost when aggregating vertices across large regions (ROI), which results in a ROI based morphometricity 3 to 20 times lower than the vertex-based morphometricity (Figure 1), similar to what we have reported on the UK Biobank (Couvy-Duchesne, Strike, et al. 2020). In addition, each atlas used to define the ROIs (here we used Desikan-Killiany) removes signal of interest in specific part(s) of the brain (Fürtjes et al. 2023), which

likely explains why we have detected significant vertices in ROIs that did not reach significance (Figure 5, Figure S19).

In summary, ROI based analyses are best suited to association analyses in single cohorts, where statistical power remains limited. However, they provide a simplified, and limited description of the associations in the brain. In future, as sample sizes grow, vertex-wise analyses can unveil more complex patterns of associations and should supersede prediction accuracy achieved from ROIs. Our results demonstrate that vertex-wise analyses can already offer a precise localisation of the brain regions associated with diseases and traits, are well powered (with samples of several thousands), and yield robust, homogeneous, and reproducible results.

In addition, our results also echo a recent debate about power of brain wide association studies. We observed that the statistical power depends on the trait studied and was larger for case control status (AD versus HC), where contrast is large, than for cognition domains (Libedinsky et al. 2022). Yet, our analysis suggests that thousands of individuals are required to detect robust associations (Marek et al. 2022), especially when the number of brain measurement tested is large (Smith and Nichols 2018), and that tens of thousands would be necessary to further progress our understanding of grey-matter structure in AD.

4.7 | GLM Versus LMM in Vertex-Wise Association Testing

Compared the current state of the art (GLM), LMM lead to parsimonious brain maps of associations (30 clusters versus 103 for AD versus HC, Tables S9 and S10), as it controls for all brain measurements (fitted as a random effect) which prevents redundant associations from reaching significance (Couvy-Duchesne et al. 2022). For proof, the 30 'LMM' clusters account for the same amount of information as the 103 identified using GLM (Figure 7, Tables S12 and S13). LMM also offer a more precise localization of the associated regions, and can identify several independent signals in close vicinity when the GLM detects a single large cluster of association (Figures 4 and 5), which aligns with results from simulations (Couvy-Duchesne et al. 2022). As sample sizes grow, the power to detect smally associated regions will increase, leading to detect more redundant regions (in low correlation with associated regions) using GLM. Some of the redundant regions may even be false positive, if the correlation between brain measurements is induced by a confounding factor, such as head motion or age (Couvy-Duchesne et al. 2022). LMM could overcome these issues and help prioritise key regions of AD atrophy that can be used to build interpretable brain-based predictors or be followed up in research.

4.8 | Family History as a Proxy-Phenotype for Alzheimer's Disease

Our analysis of maternal and paternal history of Alzheimer's, conducted in clinical cohorts as well as in the UK Biobank ($N = 37{,}644$) indicated a low (almost negligible, $R^2 < 5\%$) association with grey-matter structure. This result is in line with the weak association between familial history and AD status. In the UK Biobank, the morphometricity may be further reduced due to the relatively young age of the participants (63 years old on average), consistent with reports of an age-dependent effect of APOE on the brain (Jack et al. 2015; Thompson 2020). Our results currently suggest that family history cannot be directly used as a proxy phenotype of AD, in order to boost power of brain wide association studies, unlike in GWAS (Marioni et al. 2018).

4.9 | Limitations

In neuroimaging, choices made in image processing can impact the results. We have used a simple, albeit commonly used atlas (Desikan et al. 2006) to define our ROIs, which makes our results comparable with those published by the ENIGMA consortium. Following a recent article, we can expect that more complex atlases (with more ROIs) would capture more trait variance (morphometricity), although each atlas also captures some unique signal, which makes comparison of results across atlases difficult (Fürtjes et al. 2023). In addition, we considered the most general and high-dimensional vertex-wise representation available in FreeSurfer ('fsaverage' with no smoothing applied), as we observed that it maximised the morphometricity captured in the UK Biobank (Couvy-Duchesne, Strike, et al. 2020). Our choice led to the identification of many clusters of significant vertices, but using a simpler mesh (e.g., fsaverage6 with only 40,962 vertices per hemisphere) might have resulted in increased statistical power, by reducing the multiple testing burden, while still capturing a large fraction of the morphometricity (Figure 1). Smoothing might improve the overlap of signals across individuals' maps, although it would likely reduce the association effect sizes, with an overall unclear effect on power. In general, more work is needed to guide researchers into choosing the best image processing (and software), which may vary depending on the objective of the study and the traits of interests. This concern can be extended to the choice of harmonisation procedure, when dealing with several scanners or cohorts. Here, we used covariates (e.g., site, scanner) throughout the analyses, and meta-analysed results across cohorts, which yielded robust and replicable results. Our results can serve as benchmarks for future work that would evaluate the effect of applying more advanced harmonisation techniques, such as 'combat' (Fortin et al. 2018), its extensions or even deep-learning approaches (Hu et al. 2023).

Beyond MRI processing, the method used for multiple testing comparison can also influence power. RFT can be less stringent than Bonferroni, but only on smooth surfaces/volumes (Breznik et al. 2020), where the morphometricity (hence overall power) is reduced. More work is needed to evaluate which combination of MRI processing and multiple testing maximises power. In addition, we have used vertex-wise RFT but cluster-based RFT (Breznik et al. 2020; Nichols and Hayasaka 2003) and more advanced implementations (Bowring et al. 2021) may give different results. We have not used them here, as they have only been implemented to be performed on specific set of surfaces (typically, only cortical surfaces).

Another possible limitation concerns potential heterogeneity of cohorts. While AD status was always based on a

clinical assessment (NINCDS/ADRDA, DSM-IV or ICD10 criteria, Appendix A), some cohorts used additional inclusion criteria (e.g., MMSE score threshold for dementia severity). In addition, Alzheimer's cases, were not systematically screened for other dementias, and few had known amyloid status. Fuzzy diagnoses can lead to a loss of power, or to detect brain markers associated with general dementia and less specific to Alzheimer's disease. Of note, the modalities of recruitment and the screening of the healthy controls also varied depending on the cohort (Appendix A), which can further induce variability in the results. Lastly, MCI were typically defined using the Petersen/Winblad criteria, but the definition of impairments varied across the samples (Appendix A). To ensure reporting of robust results, we used a mixed effect meta-analytic approach that models between-cohort heterogeneity, to ensure the detected associations are consistent across samples. In practice, this reduces the influence of each cohort (and its specific ascertainment and recruitment) on the results. In addition, we validated our findings using independent samples for replication, and prediction analyses. As the sample sizes grow, it will be possible to restrict the analyses to more uniform cases (e.g., screened for amyloid), and to investigate the robustness of the results across specific subgroups of interest.

Lastly, we have treated all our traits/diseases as continuous in our analyses, meaning that our reported estimates cannot be directly converted into odd-ratios (OR), or compared with results that used a logistic regression. This is because, logistic regression is not routinely implemented for LMM, and effect sizes from linear regression can be easily transformed into approximate OR (Lloyd-Jones et al. 2018).

Acknowledgements

We used R (v4.0.0 and above) for analyses not performed using OSCA (Zhang et al. 2019) and for plots. We used the colour-blind friendly R palette *viridis*, *ukbtools* to facilitate UKB phenotype manipulation, *Morpho* and *Rvcg* to identify clusters, *rgl* to generate brain plots of associations. Other packages used include, *dplyr*, *readr*, *rmarkdown*, *matrixStats*, *RcolorBrewer*, *gridExtra*, *ggplot2*, *png*, *epuRate*.

We would like to thank Allan McRae, the Institute of Molecular Bioscience (IMB) and the Research Computing Centre (RCC) IT teams at the University of Queensland for their support with high performance computing, data handling, storage and processing.

We would like to thank Jovi Leung and Regina Wu, who downloaded and processed most of the ADNI data as part of their 2018 summer internships, funded by the Institute for Molecular Biosciences (the University of Queensland).

We thank and acknowledge the work of Giovanni B. Frisoni (MD) Principal Investigator of ARWIBO, working at the University Hospitals and University of Geneva, (Geneva, Switzerland), IRCCS Fatebenefratelli, and The National Centre for Alzheimer's and Mental Diseases (Brescia, Italy). ARWIBO is the result of effort of many researchers of IRCCS Fatebenefratelli: G. Binetti, MD, Neurobiology; L. Bocchio-Chiavetto, PhD, neuropharmacology; M. Cotelli, PhD, Neuropsychology Unit; C. Minussi, PhD, Neurophysiology; M. Gennarelli, PhD, Genetic Unit; R. Ghidoni, PhD, Proteomics Unit; D. Moretti, MD, and O. Zanetti, MD, Alzheimer's Unit.

We deeply thank the Sydney Memory and Ageing Study (MAS) team which comprises Shaily Aggarwal, Alexandra Aiken, Allison Bowman, G. A. (Tony) Broe, Kim Burns, Michele de Permentier, Joula Dekker, Louise Dooley, Sarah Fairjones, Janelle Fletcher, Therese French, Cathy Foster, Emma Nugent-Cleary-Fox, Chien Gooi, Evelyn Harvey, Rebekah Helyer, Sharpley Hsieh, Laura Hughes, Sarah Jacek, Mary Johnston, Angela King, Kate Maston, Donna McCade, Samantha Meeth, Eveline Milne, Angharad Moir, Ros O'rady, Kia Pfaeffli, Carine Pose, Wiebke Queisser, Laura Reuser, Amanda Rose, Zeeshan Shahnawaz, Amanda Sharpley, Claire Thompson, and Sam Wong.

Our sincere thanks to the OATS twins who have donated their time and data, as well as the OATS Collaborative Research Team. For New South Wales: Pamela Azar, Glenda Halliday, Antony Harding, Fiona Kumfor, John Kwok, Ora Lux, Jasmine Menant, Alissa Nichles, Peter Schofield, Alison Walker, Alfred Wong, Jacqueline Zhang; Queensland: Harry Beeby, Natalie Garden, Marlene Grace, Anjali Henders, Nick Martin, Katie McMahon, Daniel Park, Claire Redfern, Amanda Tovanen, Greig de Zubicaray; Victoria: Nicholas Cortes, Alex Connelly, Gihan Delmar, Christel Lemmon, Callum McDonald, Simone Mangelsdorf and Stacey Walker.

The authors thank all members of the EPAD Consortium, local EPAD LCS teams, parent cohort teams and research participants for their contributions to the development, setting up and running of the study.

We also thank the IT experts from the dementia plateform UK, and the Swansea university medical school, in particular Mark Newbury, Emma Squires and Catrin Morris, for their help with the High-Performance Cluster over in Swansea, Wales, which made possible to analyse the MEMENTO cohort. Open access publishing facilitated by The University of Queensland, as part of the Wiley - The University of Queensland agreement via the Council of Australian University Librarians.

Disclosure

OC reports having received consulting fees from AskBio and Therapanacea, and that his laboratory has received grants (paid to the institution) from Qynapse. Members from his laboratory have co-supervised a PhD thesis with Qynapse. OC's spouse was an employee of myBrainTechnologies. OC holds a patent registered at the International Bureau of the World Intellectual Property Organization (PCT/IB2016/0526993, Schiratti J-B, Allassonniere S, Colliot O, Durrleman S, A method for determining the temporal progression of a biological phenomenon and associated methods and devices).

PSS served on the advisory committees for Biogen Australia and Roche Australia in 2020 and 2021.

FB is part of the steering committee or Data Safety Monitoring Board member for Biogen, Merck, ATRI/ACTC and Prothena. Consultant for Roche, Celltrion, Rewind Therapeutics, Merck, IXICO, Jansen, Combinostics. FB has research agreements with Merck, Biogen, GE Healthcare, Roche. Co-founder and shareholder of Queen Square Analytics LTD.

Ethics Statement

Procedures are controlled by a dedicated Ethics and Guidance Council (http://www.ukbiobank.ac.uk/ethics), with the Ethics and Governance Framework available at https://www.ukbiobank.ac.uk/media/0xsbmfmw/egf.pdf. IRB approval was also obtained from the North West Multi-centre Research Ethics Committee. This research has been conducted using the UK Biobank Resource under Application Number 12505.

The AIBL study was approved by the institutional ethics committees of Austin Health, St Vincent's Health, Hollywood Private Hospital and Edith Cowan University.

MAS Ethics approval was obtained from the Human Research Ethics Committees of the University of New South Wales and the South-Eastern Sydney and Illawarra Area Health Service.

The MEMENTO Cohort study protocol received approval from the ethics committee 'CPP Sud-Ouest et Outre-Mer III'. The study was registered at ClinicalTrials.gov (NCT01926249). A written informed consent was obtained from all participants.

The Older Australian Twins Study (OATS) obtained approval from the ethics committees of the Australian Twin Registry, University of New South Wales, University of Melbourne, Queensland Institute of Medical Research, University of Queensland, and the South-Eastern Sydney & Illawarra Area Health Service.

The PISA study has approval from the Human Research Ethics Committees (HREC) of QIMR Berghofer Medical Research Institute and the University of Queensland.

Consent

All necessary patient/participant written consent has been obtained and the appropriate institutional forms have been archived by the data-collection teams.

In particular, informed consent was obtained from all UK Biobank participants.

Conflicts of Interest

The authors declare no conflicts of interest.

Data Availability Statement

Data used in the manuscript are held and distributed by the relevant data-managing teams, and is available upon request to all interested researchers. The summary statistics of association and the code of all analyses in a dedicated github repository are available at (https://github.com/baptisteCD).

References

Alfaro-Almagro, F., P. McCarthy, S. Afyouni, et al. 2021. "Confound Modelling in UK Biobank Brain Imaging." *NeuroImage* 224: 117002. https://doi.org/10.1016/j.neuroimage.2020.117002.

Ansart, M., S. Epelbaum, G. Bassignana, et al. 2021. "Predicting the Progression of Mild Cognitive Impairment Using Machine Learning: A Systematic, Quantitative and Critical Review." *Medical Image Analysis* 67: 101848. https://doi.org/10.1016/j.media.2020.101848.

Apostolova, L. G. 2016. "Alzheimer Disease." *CONTINUUM: Lifelong Learning in Neurology* 22, no. 2 Dementia: 419–434. https://doi.org/10.1212/CON.0000000000000307.

Balduzzi, S., G. Rücker, and G. Schwarzer. 2019. "How to Perform a Meta-Analysis With R: A Practical Tutorial." *Evidence-Based Mental Health* 22, no. 4: 153–160. https://doi.org/10.1136/ebmental-2019-300117.

Bejanin, A., D. R. Schonhaut, R. La Joie, et al. 2017. "Tau Pathology and Neurodegeneration Contribute to Cognitive Impairment in Alzheimer's Disease." *Brain* 140, no. 12: 3286–3300. https://doi.org/10.1093/brain/awx243.

Bowring, A., F. J. E. Telschow, A. Schwartzman, and T. E. Nichols. 2021. "Confidence Sets for Cohen's d Effect Size Images." *NeuroImage* 226: 117477. https://doi.org/10.1016/j.neuroimage.2020.117477.

Breznik, E., F. Malmberg, J. Kullberg, H. Ahlström, and R. Strand. 2020. "Multiple Comparison Correction Methods for Whole-Body Magnetic Resonance Imaging." *Journal of Medical Imaging* 7, no. 1: 014005. https://doi.org/10.1117/1.JMI.7.1.014005.

Brun, A., and L. Gustafson. 1976. "Distribution of Cerebral Degeneration in Alzheimer's Disease. A Clinico-Pathological Study." *Archiv Fur Psychiatrie Und Nervenkrankheiten* 223, no. 1: 15–33. https://doi.org/10.1007/BF00367450.

Choo, I. H., D. Y. Lee, J. S. Oh, et al. 2010. "Posterior Cingulate Cortex Atrophy and Regional Cingulum Disruption in Mild Cognitive Impairment and Alzheimer's Disease." *Neurobiology of Aging* 31, no. 5: 772–779. https://doi.org/10.1016/j.neurobiolaging.2008.06.015.

Chételat, G., V. L. Villemagne, P. Bourgeat, et al. 2010. "Relationship Between Atrophy and Beta-Amyloid Deposition in Alzheimer Disease." *Annals of Neurology* 67, no. 3: 317–324. https://doi.org/10.1002/ana.21955.

Couvy-Duchesne, B., L. T. Strike, F. Zhang, et al. 2020. "A Unified Framework for Association and Prediction From Vertex-Wise Grey-Matter Structure." *Human Brain Mapping* 41: 4062–4076.

Couvy-Duchesne, B., F. Zhang, K. E. Kemper, et al. 2020. "Linear Mixed Models Minimise False Positive Rate and Enhance Precision of Mass Univariate Vertex-Wise Analyses of Grey-Matter." In *2020 IEEE 17th International Symposium on Biomedical Imaging (ISBI)*, 404–407. Piscataway, New Jersey: IEEE. https://doi.org/10.1109/ISBI45749.2020.9098719.

Couvy-Duchesne, B., F. Zhang, K. E. Kemper, et al. 2022. "Parsimonious Model for Mass-Univariate Vertexwise Analysis." *Journal of Medical Imaging* 9, no. 5: 052404. https://doi.org/10.1117/1.JMI.9.5.052404.

Couvy-Duchesne, B., F. Zhang, K. E. Kemper, et al. 2021. "Association and Prediction of Phenotypic Traits from Neuroimaging Data Using a Multi-Component Mixed Model Excluding the Target Vertex." In *Medical Imaging 2021: Image Processing* 11596, 115960H. https://doi.org/10.1117/12.2581022.

de Flores, R., R. La Joie, and G. Chételat. 2015. "Structural Imaging of Hippocampal Subfields in Healthy Aging and Alzheimer's Disease." *Neuroscience* 309: 29–50. https://doi.org/10.1016/j.neuroscience.2015.08.033.

de Jong, L. W., K. van der Hiele, I. M. Veer, et al. 2008. "Strongly Reduced Volumes of Putamen and Thalamus in Alzheimer's Disease: An MRI Study." *Brain* 131, no. 12: 3277–3285. https://doi.org/10.1093/brain/awn278.

de Jong, L. W., Y. Wang, L. R. White, B. Yu, M. A. van Buchem, and L. J. Launer. 2012. "Ventral Striatal Volume Is Associated With Cognitive Decline in Older People: A Population Based MR-Study." *Neurobiology of Aging* 33, no. 2: 424.e1–424.e10. https://doi.org/10.1016/j.neurobiolaging.2010.09.027.

Desikan, R. S., F. Ségonne, B. Fischl, et al. 2006. "An Automated Labeling System for Subdividing the Human Cerebral Cortex on MRI Scans Into Gyral Based Regions of Interest." *NeuroImage* 31, no. 3: 968–980. https://doi.org/10.1016/j.neuroimage.2006.01.021.

Dufouil, C., B. Dubois, B. Vellas, et al. 2017. "Cognitive and Imaging Markers in Non-Demented Subjects Attending a Memory Clinic: Study Design and Baseline Findings of the MEMENTO Cohort." *Alzheimer's Research & Therapy* 9, no. 1: 67. https://doi.org/10.1186/s13195-017-0288-0.

Ellis, K. A., A. I. Bush, D. Darby, et al. 2009. "The Australian Imaging, Biomarkers and Lifestyle (AIBL) Study of Aging: Methodology and Baseline Characteristics of 1112 Individuals Recruited for a Longitudinal Study of Alzheimer's Disease." *International Psychogeriatrics* 21, no. 4: 672–687. https://doi.org/10.1017/S1041610209009405.

Fortin, J.-P., N. Cullen, Y. I. Sheline, et al. 2018. "Harmonization of Cortical Thickness Measurements Across Scanners and Sites." *NeuroImage* 167: 104–120. https://doi.org/10.1016/j.neuroimage.2017.11.024.

Fischl, B. 2012. "FreeSurfer." *NeuroImage* 62, no. 2: 774–781. https://doi.org/10.1016/j.neuroimage.2012.01.021.

Fratiglioni, L., and H.-X. Wang. 2007. "Brain Reserve Hypothesis in Dementia." *Journal of Alzheimer's Disease* 12, no. 1: 11–22. https://doi.org/10.3233/jad-2007-12103.

Frisoni, G. B., N. C. Fox, C. R. Jack, P. Scheltens, and P. M. Thompson. 2010. "The Clinical Use of Structural MRI in Alzheimer Disease." *Nature Reviews. Neurology* 6, no. 2: 67–77. https://doi.org/10.1038/nrneurol.2009.215.

Frisoni, G. B., R. Ganzola, E. Canu, et al. 2008. "Mapping Local Hippocampal Changes in Alzheimer's Disease and Normal Ageing With MRI at 3 Tesla." *Brain* 131, no. 12: 3266–3276. https://doi.org/10.1093/brain/awn280.

Frisoni, G. B., J. L. Molinuevo, D. Altomare, et al. 2020. "Precision Prevention of Alzheimer's and Other Dementias: Anticipating Future Needs in the Control of Risk Factors and Implementation of Disease-Modifying Therapies." *Alzheimer's & Dementia: The Journal of the Alzheimer's Association* 16, no. 10: 1457–1468. https://doi.org/10.1002/alz.12132.

Frisoni, G. B., M. Lorenzi, A. Caroli, N. Kemppainen, K. Någren, and J. O. Rinne. 2009. "In Vivo Mapping of Amyloid Toxicity in Alzheimer Disease." *Neurology* 72, no. 17: 1504–1511. https://doi.org/10.1212/WNL.0b013e3181a2e896.

Fürtjes, A. E., J. H. Cole, B. Couvy-Duchesne, and S. J. Ritchie. 2023. "A Quantified Comparison of Cortical Atlases on the Basis of Trait Morphometricity." *Cortex* 158: 110–126. https://doi.org/10.1016/j.cortex.2022.11.001.

Grill-Spector, K., Z. Kourtzi, and N. Kanwisher. 2001. "The Lateral Occipital Complex and Its Role in Object Recognition." *Vision Research* 41, no. 10: 1409–1422. https://doi.org/10.1016/S0042-6989(01)00073-6.

Guo, C., D. Wen, Y. Zhang, et al. 2022. "Amyloid-β Oligomers in the Nucleus Accumbens Decrease Motivation via Insertion of Calcium-Permeable AMPA Receptors." *Molecular Psychiatry* 27, no. 4: 4. https://doi.org/10.1038/s41380-022-01459-0.

Gutman, B. A., S. K. Madsen, A. W. Toga, and P. M. Thompson. 2013. "A Family of Fast Spherical Registration Algorithms for Cortical Shapes." In *Multimodal Brain Image Analysis*, edited by L. Shen, T. Liu, P.-T. Yap, H. Huang, D. Shen, and C.-F. Westin, 246–257. Springer International Publishing.

Gutman, B. A., Y. Wang, P. Rajagopalan, A. W. Toga, and P. A. Thompson. 2012. "Shape Matching with Medial Curves and 1-D Group-Wise Registration." *2012 9th IEEE International Symposium on Biomedical Imaging (ISBI)*: 716–719. https://doi.org/10.1109/ISBI.2012.6235648.

Hu, F., A. A. Chen, H. Horng, et al. 2023. "Image Harmonization: A Review of Statistical and Deep Learning Methods for Removing Batch Effects and Evaluation Metrics for Effective Harmonization." *NeuroImage* 274: 120125. https://doi.org/10.1016/j.neuroimage.2023.120125.

Jack, C. R., D. S. Knopman, W. J. Jagust, et al. 2010. "Hypothetical Model of Dynamic Biomarkers of the Alzheimer's Pathological Cascade." *Lancet Neurology* 9, no. 1: 119–128. https://doi.org/10.1016/S1474-4422(09)70299-6.

Jack, C. R., Jr., H. J. Wiste, S. D. Weigand, et al. 2015. "Age, Sex, and APOE ε4 Effects on Memory, Brain Structure, and β-Amyloid Across the Adult Life Span." *JAMA Neurology* 72, no. 5: 511–519. https://doi.org/10.1001/jamaneurol.2014.4821.

Jacobs, H. I. L., M. P. J. Van Boxtel, J. Jolles, F. R. J. Verhey, and H. B. M. Uylings. 2012. "Parietal Cortex Matters in Alzheimer's Disease: An Overview of Structural, Functional and Metabolic Findings." *Neuroscience & Biobehavioral Reviews* 36, no. 1: 297–309. https://doi.org/10.1016/j.neubiorev.2011.06.009.

Johnson, K. A., N. C. Fox, R. A. Sperling, and W. E. Klunk. 2012. "Brain Imaging in Alzheimer Disease." *Cold Spring Harbor Perspectives in Medicine* 2, no. 4: a006213. https://doi.org/10.1101/cshperspect.a006213.

Kochan, N. A., M. J. Slavin, H. Brodaty, et al. 2010. "Effect of Different Impairment Criteria on Prevalence of "Objective" Mild Cognitive Impairment in a Community Sample." *American Journal of Geriatric Psychiatry* 18, no. 8: 711–722. https://doi.org/10.1097/JGP.0b013e3181d6b6a9.

Koncz, R., A. Mohan, L. Dawes, et al. 2018. "Incidental Findings on Cerebral MRI in Twins: The Older Australian Twins Study." *Brain Imaging and Behavior* 12, no. 3: 860–869. https://doi.org/10.1007/s11682-017-9747-2.

Laansma, M. A., J. K. Bright, S. Al-Bachari, et al. 2021. "International Multicenter Analysis of Brain Structure Across Clinical Stages of Parkinson's Disease." *Movement Disorders: Official Journal of the Movement Disorder Society* 36, no. 11: 2583–2594. https://doi.org/10.1002/mds.28706.

LaMontagne, P. J., S. Keefe, W. Lauren, et al. 2018. "OASIS-3: Longitudinal Neuroimaging, Clinical and Cognitive Dataset for Normal Aging and Alzheimer's Disease." *Alzheimer's & Dementia: The Journal of the Alzheimer's Association* 14, no. 7: P1097. https://doi.org/10.1016/j.jalz.2018.06.1439.

Lehmann, M., J. D. Rohrer, M. J. Clarkson, et al. 2010. "Reduced Cortical Thickness in the Posterior Cingulate Gyrus Is Characteristic of Both Typical and Atypical Alzheimer's Disease." *Journal of Alzheimer's Disease* 20, no. 2: 587–598. https://doi.org/10.3233/JAD-2010-1401.

Lerch, J. P., J. C. Pruessner, A. Zijdenbos, H. Hampel, S. J. Teipel, and A. C. Evans. 2005. "Focal Decline of Cortical Thickness in Alzheimer's Disease Identified by Computational Neuroanatomy." *Cerebral Cortex (New York, N.Y.: 1991)* 15, no. 7: 995–1001. https://doi.org/10.1093/cercor/bhh200.

Libedinsky, I., K. Helwegen, U. Dannlowski, et al. 2022. "Reproducibility of Neuroimaging Studies of Brain Disorders With Hundreds-Not Thousands-Of Participants" (p. 2022.07.05.498443). bioRxiv. https://doi.org/10.1101/2022.07.05.498443.

Lindroth, H., V. A. Nair, C. Stanfield, et al. 2019. "Examining the Identification of Age-Related Atrophy Between T1 and T1 + T2-FLAIR Cortical Thickness Measurements." *Scientific Reports* 9, no. 1: 11288. https://doi.org/10.1038/s41598-019-47294-2.

Lloyd-Jones, L. R., M. R. Robinson, J. Yang, and P. M. Visscher. 2018. "Transformation of Summary Statistics From Linear Mixed Model Association on All-or-None Traits to Odds Ratio." *Genetics* 208, no. 4: 1397–1408. https://doi.org/10.1534/genetics.117.300360.

Lombardi, G., G. Crescioli, E. Cavedo, et al. 2020. "Structural Magnetic Resonance Imaging for the Early Diagnosis of Dementia due to Alzheimer's Disease in People With Mild Cognitive Impairment." *Cochrane Database of Systematic Reviews* 3: CD009628. https://doi.org/10.1002/14651858.CD009628.pub2.

Lorenzini, L., S. Ingala, A. M. Wink, et al. 2021. "The European Prevention of Alzheimer's Dementia (EPAD) MRI Dataset and Processing Workflow [Preprint]." *Neuroscience*. https://doi.org/10.1101/2021.09.29.462349.

Lupton, M. K., G. A. Robinson, R. J. Adam, et al. 2020. "A Prospective Cohort Study of Prodromal Alzheimer's Disease: Prospective Imaging Study of Ageing: Genes, Brain and Behaviour (PISA)." *NeuroImage: Clinical* 29: 102527. https://doi.org/10.1016/j.nicl.2020.102527.

Marek, S., B. Tervo-Clemmens, F. J. Calabro, et al. 2022. "Reproducible Brain-Wide Association Studies Require Thousands of Individuals." *Nature* 603, no. 7902: 7902. https://doi.org/10.1038/s41586-022-04492-9.

Marioni, R. E., S. E. Harris, Q. Zhang, et al. 2018. "GWAS on Family History of Alzheimer's Disease." *Translational Psychiatry* 8, no. 1: 1. https://doi.org/10.1038/s41398-018-0150-6.

Matsuda, H. 2016. "MRI Morphometry in Alzheimer's Disease." *Ageing Research Reviews* 30: 17–24. https://doi.org/10.1016/j.arr.2016.01.003.

Miller, K. L., F. Alfaro-Almagro, N. K. Bangerter, et al. 2016. "Multimodal Population Brain Imaging in the UK Biobank Prospective Epidemiological Study." *Nature Neuroscience* 19, no. 11: 11. https://doi.org/10.1038/nn.4393.

Minoshima, S., N. L. Foster, and D. E. Kuhl. 1994. "Posterior Cingulate Cortex in Alzheimer's Disease." *Lancet* 344, no. 8926: 895. https://doi.org/10.1016/S0140-6736(94)92871-1.

Nichols, T., and S. Hayasaka. 2003. “Controlling the Familywise Error Rate in Functional Neuroimaging: A Comparative Review.” *Statistical Methods in Medical Research* 12, no. 5: 419–446. https://doi.org/10.1191/0962280203sm341ra.

Raslau, F. D., I. T. Mark, A. P. Klein, J. L. Ulmer, V. Mathews, and L. P. Mark. 2015. “Memory Part 2: The Role of the Medial Temporal Lobe.” *AJNR. American Journal of Neuroradiology* 36, no. 5: 846–849. https://doi.org/10.3174/ajnr.A4169.

Riello, R., F. Sabattoli, A. Beltramello, et al. 2005. “Brain Volumes in Healthy Adults Aged 40 Years and Over: A Voxel-Based Morphometry Study.” *Aging Clinical and Experimental Research* 17, no. 4: 329–336. https://doi.org/10.1007/BF03324618.

Ritchie, C. W., G. Muniz-Terrera, M. Kivipelto, A. Solomon, B. Tom, and J. L. Molinuevo. 2020. “The European Prevention of Alzheimer's Dementia (EPAD) Longitudinal Cohort Study: Baseline Data Release V500.0.” *Journal of Prevention of Alzheimer's Disease* 7, no. 1: 8–13. https://doi.org/10.14283/jpad.2019.46.

Roshchupkin, G. V., B. A. Gutman, M. W. Vernooij, et al. 2016. “Heritability of the Shape of Subcortical Brain Structures in the General Population.” *Nature Communications* 7, no. 1: 13738. https://doi.org/10.1038/ncomms13738.

Sabuncu, M. R., T. Ge, A. J. Holmes, et al. 2016. “Morphometricity as a Measure of the Neuroanatomical Signature of a Trait.” *Proceedings of the National Academy of Sciences* 113, no. 39: E5749–E5756. https://doi.org/10.1073/pnas.1604378113.

Sachdev, P. S., H. Brodaty, S. Reppermund, et al. 2010. “The Sydney Memory and Ageing Study (MAS): Methodology and Baseline Medical and Neuropsychiatric Characteristics of an Elderly Epidemiological Non-Demented Cohort of Australians Aged 70–90 Years.” *International Psychogeriatrics* 22, no. 8: 1248–1264. https://doi.org/10.1017/S1041610210001067.

Sachdev, P. S., A. Lammel, J. N. Trollor, et al. 2009. “A Comprehensive Neuropsychiatric Study of Elderly Twins: The Older Australian Twins Study.” *Twin Research and Human Genetics: The Official Journal of the International Society for Twin Studies* 12, no. 6: 573–582. https://doi.org/10.1375/twin.12.6.573.

Sachdev, P. S., T. Lee, W. Wen, et al. 2013. “The Contribution of Twins to the Study of Cognitive Ageing and Dementia: The Older Australian Twins Study.” *International Review of Psychiatry (Abingdon, England)* 25, no. 6: 738–747. https://doi.org/10.3109/09540261.2013.870137.

Schuff, N., N. Woerner, L. Boreta, et al. 2009. “MRI of Hippocampal Volume Loss in Early Alzheimer's Disease in Relation to ApoE Genotype and Biomarkers.” *Brain* 132, no. 4: 1067–1077. https://doi.org/10.1093/brain/awp007.

Smith, S. M., and T. E. Nichols. 2018. “Statistical Challenges in “Big Data” Human Neuroimaging.” *Neuron* 97, no. 2: 263–268. https://doi.org/10.1016/j.neuron.2017.12.018.

Solomon, A., M. Kivipelto, J. L. Molinuevo, B. Tom, C. W. Ritchie, and EPAD Consortium. 2019. “European Prevention of Alzheimer's Dementia Longitudinal Cohort Study (EPAD LCS): Study Protocol.” *BMJ Open* 8, no. 12: e021017. https://doi.org/10.1136/bmjopen-2017-021017.

Tanaka, K. 2001. “Temporal Lobe.” In *International Encyclopedia of the Social & Behavioral Sciences*, edited by N. J. Smelser and P. B. Baltes, 15595–15599. Oxford, UK: Pergamon. https://doi.org/10.1016/B0-08-043076-7/03469-0.

Thompson, P. M. 2020. “Imaging Genomics in the ENIGMA Consortium.” *Alzheimer's & Dementia* 16, no. S4: e037325. https://doi.org/10.1002/alz.037325.

Thompson, P. M., N. Jahanshad, C. R. K. Ching, et al. 2020. “ENIGMA and Global Neuroscience: A Decade of Large-Scale Studies of the Brain in Health and Disease Across More Than 40 Countries.” *Translational Psychiatry* 10, no. 1: 1–28. https://doi.org/10.1038/s41398-020-0705-1.

Tsang, R. S. M., P. S. Sachdev, S. Reppermund, et al. 2013. “Sydney Memory and Ageing Study: An Epidemiological Cohort Study of Brain Ageing and Dementia.” *International Review of Psychiatry (Abingdon, England)* 25, no. 6: 711–725. https://doi.org/10.3109/09540261.2013.860890.

van Dyck, C. H., C. J. Swanson, P. Aisen, et al. 2023. “Lecanemab in Early Alzheimer's Disease.” *New England Journal of Medicine* 388, no. 1: 9–21. https://doi.org/10.1056/NEJMoa2212948.

van Oostveen, W. M., and E. C. M. de Lange. 2021. “Imaging Techniques in Alzheimer's Disease: A Review of Applications in Early Diagnosis and Longitudinal Monitoring.” *International Journal of Molecular Sciences* 22, no. 4: 4. https://doi.org/10.3390/ijms22042110.

Veroniki, A. A., D. Jackson, W. Viechtbauer, et al. 2016. “Methods to Estimate the Between-Study Variance and Its Uncertainty in Meta-Analysis.” *Research Synthesis Methods* 7, no. 1: 55–79. https://doi.org/10.1002/jrsm.1164.

Vijayakumar, A., and A. Vijayakumar. 2012. “Comparison of Hippocampal Volume in Dementia Subtypes.” *ISRN Radiology* 2013: 174524. https://doi.org/10.5402/2013/174524.

Villemagne, V. L., S. Burnham, P. Bourgeat, et al. 2013. “Amyloid β Deposition, Neurodegeneration, and Cognitive Decline in Sporadic Alzheimer's Disease: A Prospective Cohort Study.” *Lancet Neurology* 12, no. 4: 357–367. https://doi.org/10.1016/S1474-4422(13)70044-9.

Zhang, J., L. Xie, C. Cheng, et al. 2023. “Hippocampal Subfield Volumes in Mild Cognitive Impairment and Alzheimer's Disease: A Systematic Review and Meta-Analysis.” *Brain Imaging and Behavior* 17, no. 6: 778–793. https://doi.org/10.1007/s11682-023-00804-3.

Zhang, F., W. Chen, Z. Zhu, et al. 2019. “OSCA: A Tool for Omic-Data-Based Complex Trait Analysis.” *Genome Biology* 20, no. 1: 107. https://doi.org/10.1186/s13059-019-1718-z.

Supporting Information

Additional supporting information can be found online in the Supporting Information section.